Tufts University

3D Printed Silk Scaffolds with Riboflavin-Induced Light Curing

A thesis submitted by

ROBERT GIFFORD

in partial fulfillment of the requirements for the degree of

MASTER OF SCIENCE

in

BIOMEDICAL ENGINEERING

May 22, 2016

Advisor: Fiorenzo Omenetto

TUFTS UNIVERSITY

Abstract

Department of Biomedical Engineering
School of Engineering

Master of Science

3D Printed Silk Scaffolds with Riboflavin-Induced Light Curing

By Robert Gifford

3D printing opens up new possibilities and techniques for individualized medicine but it also comes with inherent weaknesses. One of these drawbacks is the mechanical weakness of the structures as a result of their laminar construction. This work describes a new printing system for silk hydrogels that are stiffer than any that have been printed before, paving the way for taller structures that have smaller features. As part of this printing system, a larger printer was designed with self-contained sterility systems and a greatly increased print volume compared to current models. Additionally, light-curable inks were formulated, tested, and printed using existing 3D printers to quantify their usefulness as part of a catalogue of silk-based hydrogel inks. The long-term goal for this catalogue is to document formulae and procedures that produce hydrogels of varying mechanical and biological properties for tissue engineering. The experimental procedures presented here indicate that modest amounts of physiologically inert light are sufficient to significantly increase the stiffness of riboflavin-infused silk hydrogels. In one experiment, approximately 750J of blue light increased the young's modulus of gels by 50% from 5kPa to

7.5kPa. In a printed tower test, 5J of violet light increased the modulus of plastic deformation by 13% from 15kPa to 17kPa. Single filaments made from printed hydrogels treated with focused laser light at levels below 10mJ showed no significant increase in tensile strength, suggesting that the minimum threshold for noticeable effects in 2mM riboflavin gels is on the order of magnitude of 1-5J of light. Applying more than 1,000J of light was not found to increase the stiffness of these gels. Lastly, the current uses and the future of this technology are discussed.

Acknowledgements

First and foremost I would like to thank the many exceptional mentors I have had while working at Tufts. Professors David Kaplan and Fiorenzo Omenetto were invaluable resources to me at every stage of my collegiate education. I would like to give a special thank you to Professor Irene Georgakoudi, who made it possible for me to begin my graduate studies at Tufts a year earlier than I expected. For the last three years I have always been able to count on the sage advice of Dr. Rosalyn Abbott whenever I needed it. Maria Rodriguez, Matthew Applegate, and Bradley Napier continuously provided me with advice and expertise as I worked on this project. Similarly, Lauren Baugh and Yuqi Wang from the Black Lab helped me immensely by performing AFM measurements and MatLab analysis. Gyde Lund and Adrian Chu worked very hard putting together the 3D printer designed as part of this project. Thank you, Sara Watson, James Gifford, and Elise Gifford, for supporting me from the very beginning. Last but certainly not least, Dr. Joseph Brown, Dr. Mark Brenckle, and Mark Paquette all helped me grow as a scientist during my time at Tufts. This work was made possible with funding from the Silk Lab at Tufts University.

Contents

Abstract……..……...….*ii*
Acknowledgements…….....*iv*
List of Figures…….*vii*
List of Tables……..…….…*ix*

1.0 Background……..*1*
1.1 The origins of 3D Printing…….....*1*
1.2 RepRap and Custom 3D Printers……...*3*
1.3 Current State of the Art……....*5*
1.3.1 Light Sources for Stereolithography……*6*
1.3.2 Hydrogel Photoinitiators……...*9*
1.3.3 Printable Hydrogels……..*11*
1.3.4 Novel Design Opportunities……....*14*
1.4 3D Imaging……*15*

2.0 Designing the 3D Printer……..*18*
2.1 Sterility……...*18*
2.1.1 Airflow ……*18*
2.1.2 Ultraviolet Applications……....*21*
2.2 Electronic Controls……..*22*
2.3 Software…….....*23*

3.0 Printable Biomaterials……..*25*
3.1 Earlier Gels……...*25*
3.2 UV Curable Inks……...*27*
3.2.1 Mechanism of Light Curing……..*27*
3.2.2 Ink Formulation Methods……....*29*
3.2.3 Experimental Gel Conditions ……*32*
3.3 Print-Time Stability……*34*
3.4 Viscosity……....*36*
3.5 Gel Characterizations ……*36*
3.5.1 Compressive Strength……...*37*
3.5.2 Tensile Strength ……*46*
3.5.3 AFM Probing ……*50*
3.5.4 Printable Tower Stiffness...……...*52*
3.6 Discussion ……*54*

4.0 Current Applications……..*62*
4.1 3D Printed Tissue Replacements……*62*
4.2 Limitations of Available Printers……...*64*
4.3 Dynamic Elasticity Implants……*65*

5.0 Future Directions……*67*
5.1 Biocompatibility Investigations……..*67*
5.2 3D Printed Organ Replacements……..*70*
5.3 3D Printing in the Millimeter and Meter Scales……..*72*

Appendix A……..*74*
Appendix B……..*75*
Appendix C……..*76*
Bibliography…….....*77*

List of Figures

1. A representation of stereolithography…….....1
2. A desktop MakerBot …….....2
3. RepRapPro "Mendel" printer……4
4. Emission spectra for common lights……...8
5. Side-by-side comparison of 3D scanners……...16
6. Fasotec 3D printed surgical dummy…….....…..17
7. Annotated picture of the printer's airflow system …….....19
8. Wiring schematic of the GT2560……..…….....22
9. Repetier-Host start-up page……...24
10. Repetier-Host settings close-up……..…….....24
11. Elastic modulus of various tissues…….....26
12. Simplified riboflavin molecular structure……..…….....27
13. Simplified L-arginine molecular structure…….....27
14. Riboflavin salt hydrate molecular structure……..……..28
15. Absorbance spectra of riboflavin…….....28
16. Extruding one drop of riboflavin-infused ink…….....36
17. Biopsies from experimental condition 1……..……..38
18. Biopsies from experimental condition 2……..……...39
19. Biopsies from experimental condition 3…….....…….....40
20. Biopsies from experimental condition 4……...…….....41
21. Biopsies from experimental condition 5……..……..42
22. Biopsies from experimental condition 6……..….....43
23. Biopsies from experimental condition 7…….....44
24. Elastic moduli by experimental condition……45
25. Example of a twisted filament……...46
26. Example of a toe region in tension…….....48
27. High-contrast image of a 3D printed filament……...49
28. Surface stiffness of a laser-exposed gel……...……....51
29. Stiffness of printed tower biopsies…….....53
30. Expanded data from figure 21……...…….....55
31. Biopsy locations from experimental condition 4……55
32. Modulus over 12 cycles for biopsy 4,6,4……..……..56
33. Modulus over cycles 5-8 for gels 4,5 and 4,6……..57
34. Rerun ratio vs. cycle 5 or 6 modulus……..58
35. Gel modulus vs. biopsy height……...59
36. Biopsy 1,2,2 compression to failure……...60
37. Gel moduli from failure testing……60
38. Modulus of low outlier from cycle 5 vs. failure …….……61

39. High-end leg prosthetic from 3D Systems…….....62
40. Open Hand project……..…….63
41. Total hip replacement contents……..……....66
42. Rudimentary printed tissues…….....71
43. Large and small photolithography examples…….....72
44. Winsun Corporation concrete printer……73
45. Blue light exposure setup…….……..74
46. Gel moduli from failure testing and cycle 5 compared……...75
47. Gel moduli vs. exposure time……76

List of Tables

1. Light sources in stereolithography……6
2. Absorption peaks of photoinitiators……9
3. Printable hydrogels……12
4. Example 1mL light curable silk ink……31
5. Example experimental formulae …….…….....34
6. Demonstration of unhelpful p-values……57

1.0 Background

1.1 The origins of 3D Printing

In 1986, Charles Hull patented the first contemporary form of 3D printing and ushered in a new era of manufacturing[31]. His system, an early form of stereolithography, created laminar structures by hardening the surface layer of a fluid as its level rose inside a chamber. Shortly thereafter, Carl Deckard patented selective laser sintering (SLS), a similar process that uses a reservoir of solid metal beads instead of a fluid[21]. Before the end of the 80's, a third method of 3D printing was patented: fused deposition modeling (FDM). By far the most ubiquitous form of 3D printing today, FDM involves melting a plastic resin and extruding it onto a build plate that moves lower relative to the print head with each layer[36].

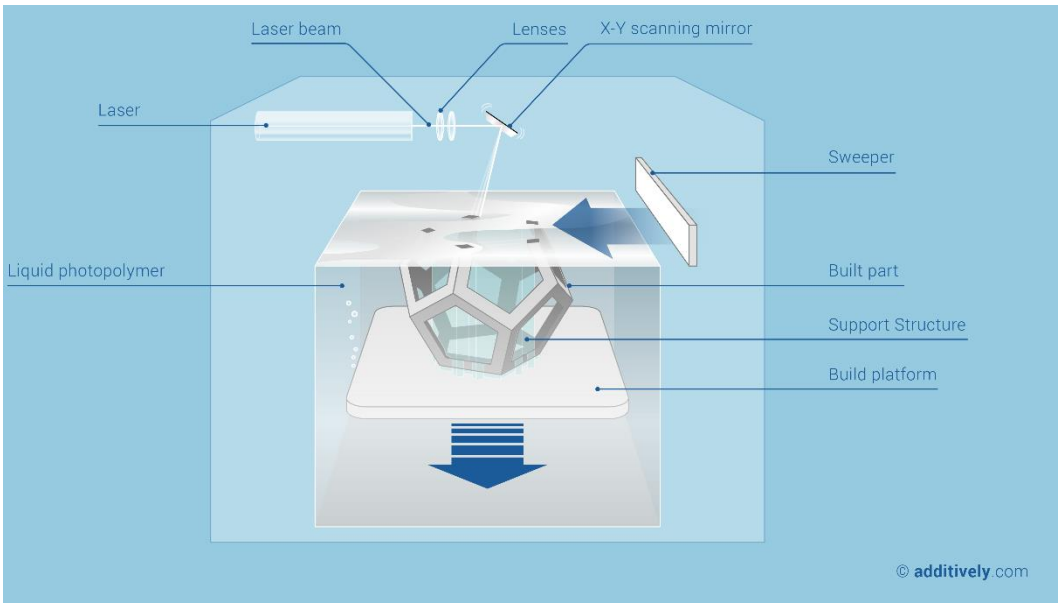

Figure 1: A representation of stereolithography showing the polymer fluid, the crosslinking light source, and the build plate. SLS operates on the same principles but with metal beads instead of a fluid. FDM directly deposits plastic in the shape of the structure. Image source: additively.com

Initially, these three technologies were developed with the goal of accelerating research and development by producing basic prototypes on demand. The term "rapid prototyping" comes from this era of industrial use, before the advent of consumer 3D printers. In the early 1990's, the field of 3D printing vastly expanded as the cost of 3D printers plummeted while computers and new techniques made their capabilities soar. Printers were being introduced that could print at ever-higher resolutions with newer, more versatile materials. Prices finally reached so-called affordable rates in 2007, with the release of "Darwin," the first product of the RepRap (short for replicating rapid prototype) project aimed at creating a 3D printer that could produce its own parts efficiently[36]. Home consumers could purchase their own RepRap printer starting in 2009, the same year that MakerBot started selling its iconic Replicator. The late 2000s were characterized by these such price wars as companies moved out from the high-end industrial market into the much larger consumer market, just as home computers did in the 1980s. Recently, the crowdfunded Peachy Printer Project passed an important milestone as it adapted SLA technology to produce "the world's first $100 3D printer" according to their website, though the $100 product comprises just the laser equipment.

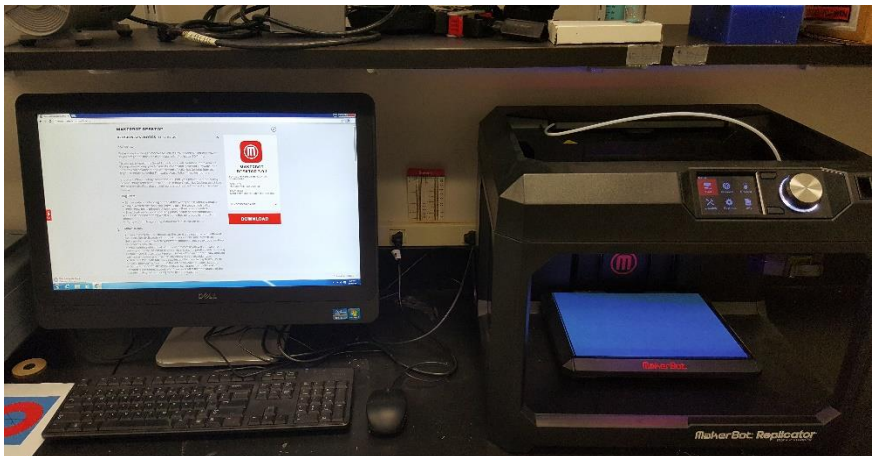

Figure 2: A MakerBot Replicator on a desktop in the Omenetto Lab.

Now thirty years old, the field of 3D printing has become ubiquitous across all areas of manufacturing and includes more than a half dozen different technologies, each with its own strengths, weaknesses, and vocabulary. Generally speaking, additive manufacturing, rapid prototyping, and freeform manufacturing are all terms for 3D printing that refer to the same group of processes and capabilities as a whole. Individual companies own the intellectual property behind labels like laser sintering, stereolithography, and fused deposition modeling, each of which comprises a segment of the $4 billion 3D printing market[70]. As new techniques and technology emerge, the capabilities and nomenclature of the industry evolve to accommodate each innovation.

1.2 RepRap and Custom 3D Printers

The RepRap project was conceived in 2004 by Adrian Bowyer as a way to accelerate the improvement of 3D printers while reducing their cost[36]. The hallmark of a RepRap printer is the ability to print most of its own parts while sourcing the remaining parts from freely available materials, such as standard framing and motherboards. The most recognizable aspect of the "free and open-source" nature of the printer is the fused filament fabrication (FFF) method, a synonym for fused deposition modeling that does not require licensing the phrase from Stratasys Inc. FFF and FDM use a thermoplastic polymer stored in a solid reservoir and driven through a heated extruder onto a cooler build plate to grow a laminar structure.

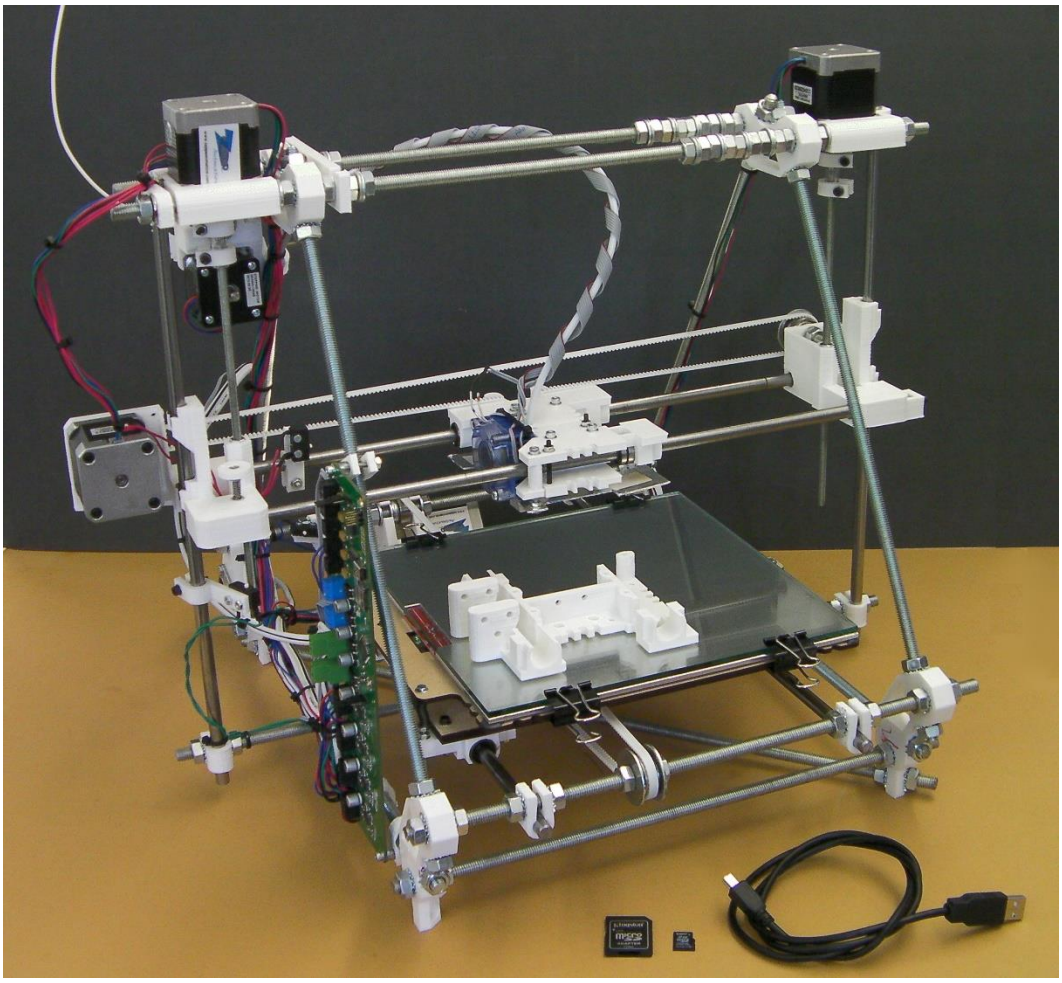

Figure 3: A RepRapPro "Mendel" model introduced in 2013 and shown printing a copy of its own extruder mount. Image source: reprap.org

RepRap printers, unlike their competitors, are meant to be upgraded by users in order to fulfill their individual needs. Bowyer imagined his printers outpacing their competitors by encouraging users to adapt small aspects of each printer and then sharing their ideas as part of a continuous open-source evolution[36]. The aftermarket value for these parts and their improved descendants exceeded the value of the plastic and energy put into them, which fulfilled Bowyer's second goal of lowering the net cost of each printer. Everyone who bought a RepRap could sell RepRap parts they printed to the next customer, and use the marginal profits from each sale to invest in improving those designs. In practice, the market for RepRap parts has

remained too small for an individual user to turn a profit, but users still continuously upgrade their machines with crowdsourced ideas[6].

1.3 Current State of the Art

The greatest strength of rapid prototypers today is their ability to create one unique, intricate structure much faster than traditional manufacturing techniques, and even faster than milling in some cases[78]. Over the last five years, researches have increasingly used this power to print exact copies of patients' organs as scaffolds for tissue replacement[16]. Hydrogels are among the most promising materials for tissue replacement because of their fluid transport properties, biocompatibility, and programmable mechanical properties[79]. The most versatile method of controlling the chemical and physical properties of these hydrogels is with using a spatially-controlled laser / photoinitiator system[73]. In this way, it is possible to control the strength of the hydrogel's macrostructure, by 3D printing it in a reinforced pattern, and its microstructure, by exposing it in some points and not in others. Consequently, this altered form of stereolithography has become a popular technique in biomedical engineering and many different procedures have been developed using a variety of light sources, photoinitiators, and printable hydrogels[74]. Most commonly, researchers have combined an ultraviolet light source with a UV-compatible photoinitiator, but this can lead to DNA damage and cell death within the scaffold[67]. The design challenge in this thesis is to create a novel, useful system of printing and stiffening hydrogels through stereolithography without using UV components or harsh organic solvents.

1.3.1 Light Sources for Stereolithography

As previously mentioned, stereolithography systems traditionally have used UV light sources because of their high energy (and therefore higher fluence) and their ubiquity. The main drawback to using UV light, even weaker UVA wavelengths, is that the amount of fluence necessary to cause gelling can cause DNA damage, leading to cell death or carcinogenesis[79]. On the other side of the visible spectrum, near-infrared light sources have been used in a very limited capacity for stereolithography[73]. Visible-wavelength stereolithography was preferred in this study because it offers a cell-compatible source of energy for chemical activation without requiring two-photon excitation. However, the selection of photoinitiators for visible light excitation is much more limited than it is for UV light.

Source Name	Type	λ	Fluence	Limitations
KrF	Pulsed Laser[12]	248nm	150kW/cm^2	Intense UVB
XeCl Excimer	Pulsed Laser[10]	308nm	1MW/cm^2	Intense UVB
Black Light	Fluorescent[16]	365nm	2mW/cm^2	Low Power UV
Our Laser	Handheld Laser	405nm	32mW/cm^2	Very Low Power
Our LEDs	LED	450nm	7.8mW/cm^2	Very Low Power
Bluephase 16	LED[44]	450nm	1.6W/cm^2	Broad Excitation
Xenon	Laser[32]	458nm	0.5W/cm^2	Narrow Band
Blue Diode	Laser[44]	474nm	35mW/cm^2	Narrow Band
Solid Diode Plotter	Laser[34]	680nm	0.38W/cm^2	Uneven Spectrum
Ti:Sapphire	Pulsed Laser[58]	800nm	-	Two-Photon
Near-IR	CW Laser[71]	808nm	1.78W/cm^2	Low-energy

Table 1: A summary of light sources used in stereolithography for hydrogel synthesis.

The table on the previous page summarizes the kind of lasers currently used in the literature to excite photoinitiators that cause gelling within hydrogel precursors. Naturally, no one source of illumination is perfectly suited for all stereolithographic processes, but very few light sources are suitable for the kinds of printing done in the Omenetto lab. Lasers, for example, often emit light within only 5-10nm of their peak wavelength, severely limiting their use to only a handful of photoinitiators each. Fluorescent lights suffer from the opposite phenomenon, emitting light across 100s of nanometers at uneven levels, making them inefficient and underpowered for most chemical processes[73]. Blue light emitting diodes fall in between these extremes, emitting light within 50nm of their peak and offering modest amounts of fluence[44]. Pulsed lasers can provide extremely high fluence (light density) with a small amount of power, but these can exceed the damage threshold the material before they cause photopolymerization[83]. While it is possible to increase or decrease the power coming from any of these light sources, any amount of UV light could cause irreparable cell damage, making these inappropriate for cell printing. Even the Ti:sapphire laser, which does not emit high-energy wavelengths, can cause cell death in the excited areas[58]. Importantly, the choice of photoinitiator is linked to the choice of light source, and the high fluence from the two-photon Ti:sapphire laser caused cell death when all the PI was rapidly converted to oxygen radicals. Consequently, the illumination sources in this study were chosen for their low cost, ease of use, visible

spectra, and compatibility with riboflavin. Compare below the emission spectra of four available light sources for photopolymerization studied in *Tehfe et al, 2013*.

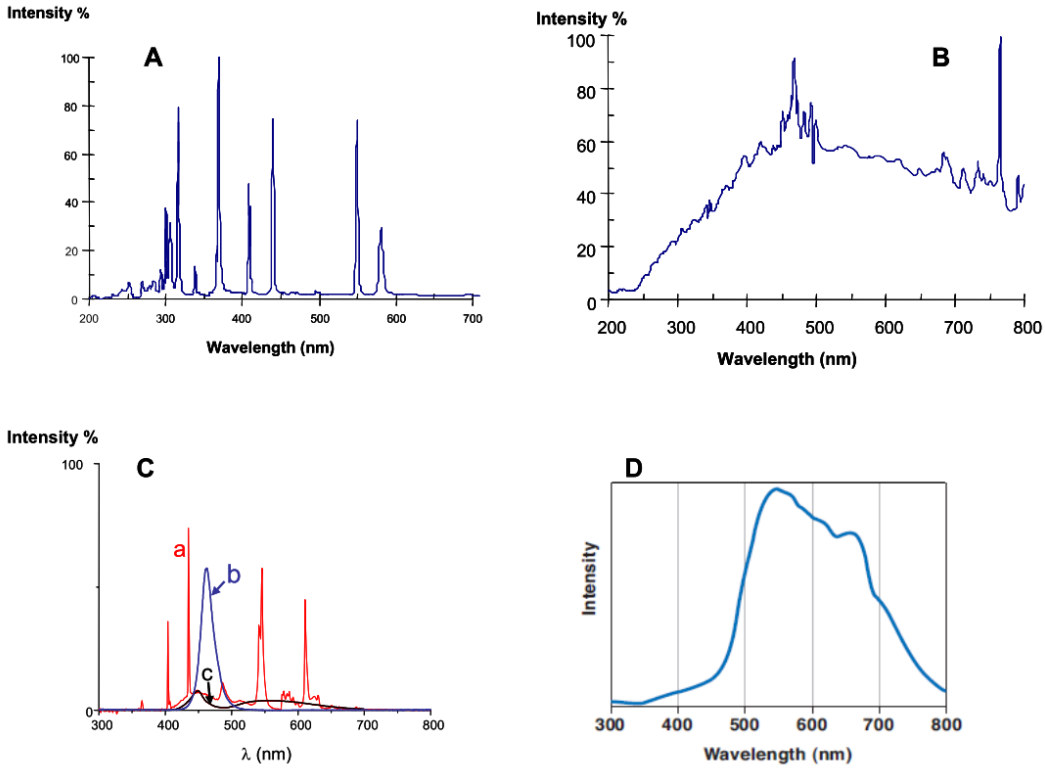

Figure 4: Emission spectra for (A) Hg-Xe lamp, (B) Xe lamp, (C) consumer lights [fluorescent bulbs {a}; blue LED {b}; white LED {c}] and (D) a halogen lamp. Image source: Tehfe, 2013.

The first, figure 4a, is a mercury-xenon lamp that covers a broad spectrum of wavelengths, but only very narrow bands at specific peaks. Figure 4b shows the spectrum for a traditional xenon lamp, with intense peaks over a broad spectrum. In figure 4c, three common household sources of household lighting are compared. Note the intense, narrow of the fluorescent bulb contrasted with the muted, broad peaks of the white LED (curves "a" and "c" respectively). The halogen lamp, on the other hand, has one peak but can emit a broad spectrum of light and favors one end of the spectrum over the other. Two- and three-photon systems can activate otherwise unattainably high-energy systems using lower-energy wavelengths[68].

1.3.2 Hydrogel Photoinitiators

Hydrogels are polymer-based gels formed from one or more precursors that are chemically bound together in order to form a sponge-like structure. One method of catalyzing this bond formation is to introduce oxygen radicals into the precursor solution. In stereolithographic processes, a photoinitiator is added in low concentrations to the solution and then excited with one of the light sources listed in the previous section. Section *3.2.1 Mechanism of Light Curing* details the specific chemistry involved in this process, but it is clear from the emission spectra in the previous figure that photoinitiators must be paired with compatible light sources to efficiently form hydrogels. Researchers can compensate for small mismatches between the light source and the photoinitiator by increasing its concentration or the fluence of the system, but most photoinitiators are limited to the UV spectrum.

Photoinitiator	Absorption peak (nm)	Typical co-initiators	Uses
Darocur 1173	250-330	-	Photoinitiator[22]
BAPO	350-380	-	Photoinitiator[12]
Irgacure 2959	260-360	-	Photoinitiator[30]
Riboflavin	370-450	L-arginine[40]	Metabolite
Our Riboflavin Salt	370-450	-	Metabolite[8]
VA-086	375	-	Photoinitiator[77]
Emax 904	<400	-	Adhesive[9]
Camphorquinone	400-500	-	Dental[47]
Rose Bengal	530	-	Toxic Photoinitiator[32]

Table 2: Representative photoinitiators and their absorption peaks. Note that the majority require UV sources and almost all absorb within the UV range.

That most photoinitiators absorb within the UV range is not surprising; shorter-wavelength photons provide more energy and development of these chemicals has rarely considered their biocompatibility. In the case of bioprinting, however, UV light is an unacceptable risk to the health of the patient who might receive carcinogenic cells in a tissue scaffold that has been exposed to UV light. For this reason, the entire Irgacure, Darocur, Emax, and Va-086 product lines, along with BAPO, are unsuitable for this printing system. While only the most commonly cited member of these chemical groups is listed above, their entire groups have similar absorption spectra. For visible light photoinitiators, the selection is much narrower and the chemicals are often less effective. Camphorquinone (CQ) is a visible-light photoinitiator used in dental applications where the layer depth is very shallow and the resulting structure is not a hydrogel but a hard, durable enamel replacement[48]. Similarly, Rose Bengal is a visible light photoinitiator, but is unusable because it has been shown to cause cell death in exposed areas[32]. Further work would be required to quench the cytotoxicity in those areas and use Rose Bengal for 3D bioprinting live cells. Clearly the availability of biocompatible photoinitiators is limited, but riboflavin and its conjugates are suitable species. With an absorption spectrum spanning from UVA light to yellow-blue[39], they can produce enough oxygen radicals to polymerize certain hydrogels even at low concentrations with modest fluencies. In cases where the level of reactive oxygen species necessary to cure the gel is high enough to cause cell death, additional oxygen can be added to quench the reaction[39], but this is not studied in this report. The reason for this counter-intuitive inhibition is that molecular oxygen is attracted to unbound oxygen radicals and reduces their reactivity by forming a more stable oxygen triplet.

1.3.3 Printable Hydrogels

The polymer that will comprise the molecular backbone of the hydrogel is often the first choice that a researcher will make, yet this decision both informs and is informed by the choice of photoinitiator and light source. In the case of silk, and especially with silk bioprinting, the photoinitiator had to be thermally stable, water-soluble, and biocompatible. Silk can be made optically transparent as necessary[8], which allows for greater flexibility when choosing a light source. Silk is adaptable both physically and chemically, meaning its mechanical and biological properties can be altered more readily than other biopolymers[41]. Building on that foundation, this work investigated how silk hydrogels could fulfill unmet needs as tissue scaffolds.

As hydrogels have become a more popular subject to study as tissue scaffolds, the methods to print and gel them have become more diverse. The result of all this research is that there are now hydrogels whose mechanical properties range more than seven orders of magnitude (see table 3). Some hydrogels only require time in order to gel[80], while others employ high-power lasers to achieve extremely stiff moduli like those found in bone[12]. Importantly, a review of the literature did not return any examples of a cell-laden hydrogel that could mimic the exact properties of a specific bodily tissue. Furthermore, the majority of reported stereolithographic systems for hydrogels used UV light as a curing agent, which would make them unsuitable for bioprinting. Even in cases where high cell viability is reported, the unknown carcinogenic factor would make these scaffolds unsuitable for implantation. There is a large unmet need for a printable hydrogel that can match the mechanical properties of native tissue with a high degree of control and without using cytotoxic processing.

Polymer(s)	Gelling Agent(s)		Modulus	Limitations
PEO/PEGDM	Irgacure 2959	UV Light	1-1.5kPa	Weak, small modulus range[23]
Alginate-HA	PEI	$CaCl_2$	1.5kPa	Small modulus range[61]
Gelatin-Elastin	-	-	2-15kPa	Modulus not spatially controlled[1]
Alginate	$CaCl_2$	IR Light	2-25kPa	Stiffening only temporary[72]
Agarose	-	-	5-20kPa	Printed sterile[3]
Alginate	$CalCl_2$	$BaCl_2$	5-30kPa	Modulus not spatially controlled[72]
PEGDA/alginate	Irgacure 2959	UV Light	5-75kPa	Cells seeded only after printing[30]
Methacrylated gelatin PEGDA/alginate	Irgacure 2959	VA-086	20-120kPa	High oxidative stress, UV light[78]
PNIPAM-gelatin	M199	UV Light	10-350kPa	Little control over the modulus[56]
Collagen	Riboflavin	Blue Light	300-700kPa	Flat structures only[62]
Alginate/Acrylamide	Emax 904	UV Light	0.3-2.7MPa	Structure is mostly adhesive[9]
PEGDMA	Irgacure 651	UV Light	4-6MPa	Rapid gelling[49]
PEG/PEGDA	BAPO	UV Light	10-13Mpa	Small modulus range[14]
Silk	-	-	20-30MPa	Modulus not spatially controlled[15]
PPF and DEF	BAPO	UV Light	6-18GPa	Flat, not biocompatible[12]

Table 3: A summary of the dominant properties for recently explored printable hydrogels. Remember that any system that uses UV light is a potential hazard to a patient who receives the scaffold.

From a strictly physical point of view, most hydrogels occupy one niche within the range of elastic moduli commonly seen in human tissue (for more on this, jump to section *3.1 Earlier Gels*). The PNIPAM-gelatin gels would seem to be more versatile than the others because their moduli span more than an order of magnitude[56]. As is commonly the case, their strength is also their greatest weakness, as the procedure

outlined in *Ohya et al* does not offer a method to control how stiff the resulting gel will be[56]. Alginate gels can be made to copy the stiffness of human tissue, but their gelling is usually controlled by the presence or absence of a salt (often $CaCl_2$) or a chelating agent[61]. However, there is no spatial control over the stiffening as is the case in a stereolithographic system. Worse still, the stiffening is temporary in the case of $CaCl_2$ because the salt eventually leeches from the hydrogel. To address these limitations, *Tabriz et al* created a 3D printer that permanently gels cell-laden Alginate in a bath of $BaCl_2$. This system is capable of printing cells directly into a printed tissue scaffold within a media bath and then permanently increasing their stiffness. The limitation of this system is that the $BaCl_2$ bath indiscriminately stiffens the structure as the chemicals bind to the alginate irreversibly[72]. In order to truly recreate physiologically relevant features, any 3D printed hydrogel will need spatially-defined properties. As such, anisotropic features cannot be replicated in this way and will require greater complexity in their design and production. One example of stereolithographic system for hydrogels is the work by Harvey Rich, which described a technique to use a visible-wavelength laser and riboflavin to selectively harden a collagen disc. Unfortunately, their collagen hydrogels needed to be compressed to 50-60μm in order to be fully exposed[62]. Obviously, there is little advantage in 3D printing tissue when it can only be 60μm tall.

Clearly, there is an opportunity for a 3D printing system that can print bio-inks in large, intricate structures with anisotropic properties. Because hydrogels provide both excellent biocompatibility and strength, it is worth investigating the potential for a silk-based hydrogel to create tissue scaffolds for organ replacement.

1.3.4 Novel Design Opportunities

It was shown in the previous three sections that the field of bioprinting has produced many promising, yet flawed, solutions to the problem of recreating native tissue. Current systems rely on harmful UV radiation or produce structures that are too dissimilar to native tissue to be viable replacements for urgently needed organs. The goal of this work will be to advance the field of tissue engineering by building, testing, and confirming the ability of a silk-based hydrogel to mimic the mechanical properties of human tissue. The resulting hydrogel will be 3D printable, biocompatible, and capable of anisotropic alterations to its properties after printing.

The printing system itself will be designed to be sterile and larger than previous bioplotters but maintain the same level of accuracy while costing less than a commercial printer. These capabilities will provide the Omenetto lab the opportunity to lead the industry in prototyping new bioinks, tissue scaffolds, and ultimately, new tissue replacement therapies. The hydrogels studied here will fit in to a larger collection of silk-based inks that can be printed and processed into physiologically relevant structures. Their novelty and utility will be determined by the final properties of the printed structures that can be made with these inks. If these hydrogels can be printed stiffer than those that came before them, it will empower researchers to build larger tissue scaffolds with smaller features more quickly than ever before. Ultimately, this thesis will serve as an outline for envisioning, producing, and characterizing hydrogels for tissue engineering at Tufts University.

As a final note on the background for this work, the next section covers the 3D imaging technology necessary to make 3D printing relevant for tissue engineering.

1.4 3D Imaging

3D imaging is the natural inverse of 3D printing, and both fields comprise a key development in personalized medicine. Whereas the former seeks to understand an object by making it virtual, the latter seeks to recreate a virtual pattern as a real object. There are innumerable advantages to medicine created by the ability to passively observe the inside of the body and recreate patient-specific geometries[63]. Innovations such as magnetic resonance imaging and optical coherence tomography have revolutionized the way doctors and patients understand their pathology[52]. For 3D printing developers, even 3D imagers that can only view the surface of an object are an invaluable link between a design and a finished product.

The first 3D scanner to be marketed to the mainstream consumer was MakerBot's Digitizer, first announced in 2013. At the time, commercially available competitors were specialized and priced above what a hobbyist could afford. Unlike an MRI or CT scan which produce a 3D volume from 2D slices[25], the Digitizer is a portable desktop device that reads the surface of an object as it turns in front of the camera. The resulting file is an editable mesh that designers can manipulate and reprint. These desktop scanners are less useful for medicine however, because they lack scanning depth and the ability to measure part or all of a patient[34]. Knowing these limitations, the next generation of scanners unchained themselves from the object.

Figure 5: On the left, a first-generation portable 3D scanner, the MakerBot Digitizer. On the right, a second generation portable scanner, the ZScanner. Images sourced from 3ders.org and engadget.com, respectively.

For the second generation of 3D scanners, a permium was placed on expanding the types of objects that could be scanned and increasing the accuracy of the scan. Improvements in these fields were made by companies such as Z Corporation, whose Z scanner (figure 4, above) does not need the scanned object to move on a plate. Because these handheld scanners are disconnected from the object, they can create models regardless of their size or shape, limited only by their depth of field and scanning rate. Other competitors in this field include the EVA 3D Scanner, which does not require markers and can capture color images, and the AMETEK line of portable scanners, which ranges from high-end surveyors to consumer handhelds. According to their websites, *artec3d.com* and *creatform3d.com*, respectively, these devices rival the surface accuracy of medical-grade equipment, but cannot match their depth of field. AutoDesk sensed this opportunity and developed 123D Catch, a smartphone app tailored to virtualizing people that creates computer models from smartphone camera photos. Any doctor with access to a smartphone and *123dapp.com* could quickly and cheaply understand a pateint's pathology, recreate it, and analyze the best treatment from across the world.

As innovative as consumer 3D scanners are getting, they still cannot visualize deep-tissue injuries that require expensive scanning equipment found only in labs. One area where 3D printing can help these patients is providing practice for surgeons facing complicated procedures. In 2008, a team lead by Stephan Jacobs studied a patient with a uniquely malformed heart who needed surgery to correct a left ventricular aneurysm and a right ventricular tumor[34]. Using MRI and CT images, the doctors studied the patient's deformity, printed a plaster copy of the heart, and then practiced for the surgery using the model to identify potential risks and difficulties.

Figure 6: Surgeons at the Kobe University Graduate School of Medicine in Japan use a 3D printed patient model from Fasotec for practice. Image source: (Millsaps, 2015)

Today, those techniques have been expanded around the world to aid in high-risk or complicated pediatric, brain, lung, or liver surgeries. One of the goals in this project was to design a system capable of reproducing the properties of living tissue, and before this technology will be used to replace organs it could be used to teach the next generation of surgeons how to perform those future surgeries.

Chapter 2 – Designing the 3D Printer

2.1 Sterility

The vast majority of commercially-available 3D printers are designed around thermoplastic and thermoset polymers whose melting points or glass transition temperatures are high enough to make them stable at room temperature. For example, the MakerBot website says that the ABS plastic used in their printers has a T_g of 105ºC (221ºF) and is extruded at 230ºC (446ºF). These temperatures are optimized for consumer use and clearly sterilize the material as it is printed, but temperatures above the boiling point of water are unsuitable for the aqueous silk-based inks used by Tufts biomedical engineers. Compounding this issue was the desire to print living cells without allowing bacteria or fungus to thrive, eliminating the possibility of printing under a radiation source to kill contaminants. It was immediately apparent that this printer would need an alternative method of sterilizing the inks that were printed.

Ultimately, a hybrid containment/UV irradiation system was implemented. While the printer is extruding living cell samples, a positive-pressure system will keep external contaminants out. In order to decontaminate the build plate before and after printing, a UV lamp was installed and a cleaning program was drafted for the motor controller to allow every part of the printer to be exposed to sterilizing light.

2.1.1 Airflow

The final design for this printer incorporates a positive-pressure laminar flow hood system similar to the one used in biosafety cabinets. First, a humidifier warms and acclimates air that has been drawn into a chamber through a particle filter. Next,

a small motor pulls the air above the printer and pushes it down through a sterile HEPA filter and into the lightly sealed printing chamber. The partial seal creates a high pressure zone within the printing chamber that forces air out through any unsealed openings, stopping the influx of airborne bacteria and fungi. Laminar flow, defined by having a low Reynold's number, requires a relatively low velocity within such a large space. The work done to characterize and build the airflow capabilities into the 3D printer was completed by Gyde Lund, an undergraduate mechanical engineering student brought on to design and assemble the printer.

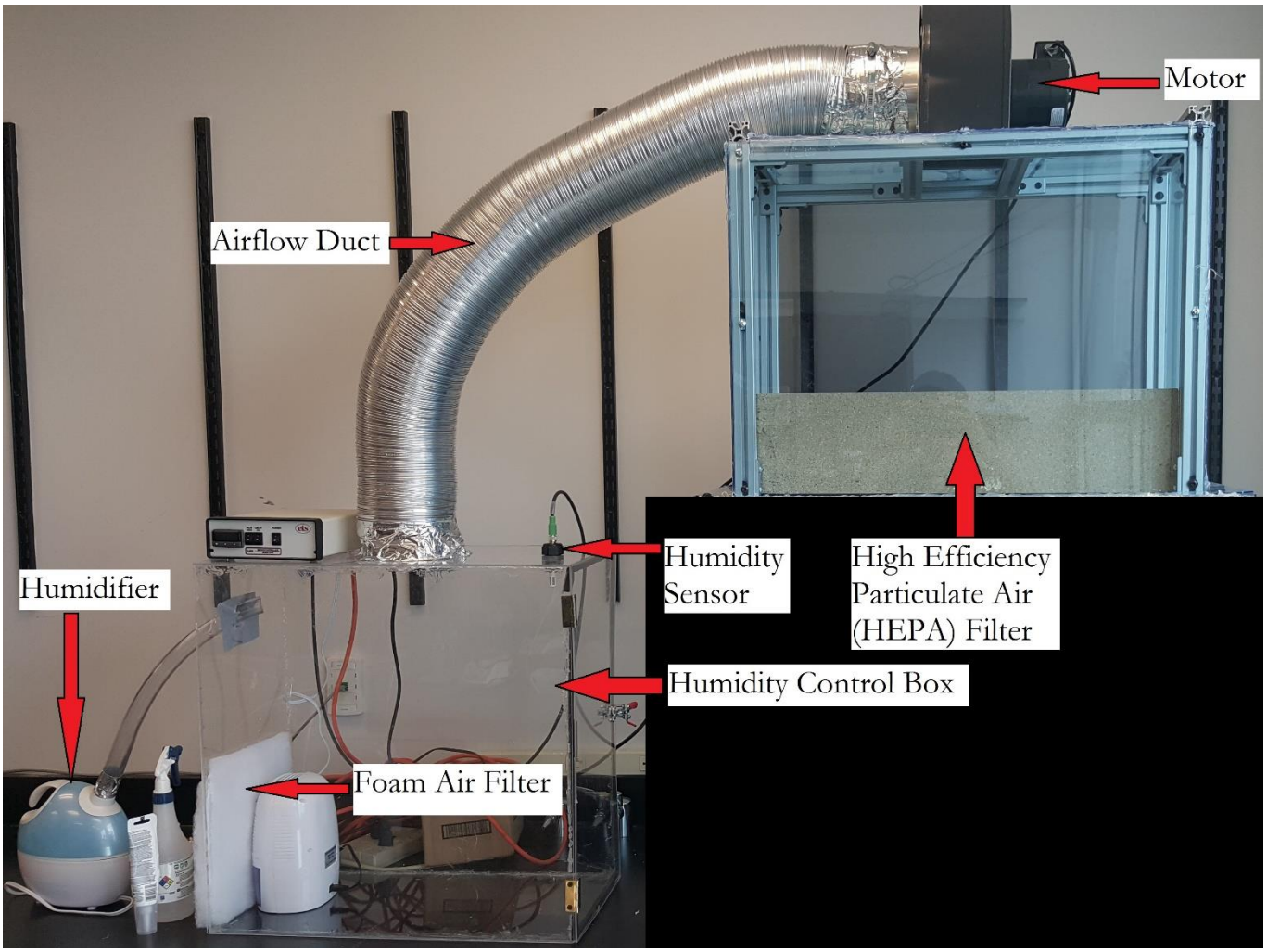

Figure 7: An annotated picture of the sterile airflow systems that protect the print area (blacked out, lower right) from contaminants.

As of this writing, no other bioplotter has its own self-contained laminar flow system. This printer, being both isolated from the outside and sustaining positive pressure around the print area, is by far the largest, most sterile printing system available to the Omenetto lab. The design of the airflow system mimics the laminar flow system of a class-II biosafety cabinet (BSC). The maximum airspeed for laminar flow is stated as 100ft/min, or 0.5m/s[9]. In both BSCs and in this printer, it is advantageous to keep the air moving as quickly as possible without introducing turbulence into the working space. Keeping the airflow laminar is critically important because it ensures that the flow lines (the paths that all airborne particles take) pass through the filter, over the print surface, and out through the bottom of the print area. Any turbulence in the print area could allow cross-contamination from one area of the printer to another, or worse, outside contaminants to flow into the printer. In order to power the laminar flow, the motor in this build spins at 1,750rpm for an output of 180ft^3/min through a 1ft-by-2ft HEPA filter surface, yielding an output velocity of 90ft/min.

While the addition of a laminar flow system addressed the design challenge of creating a sterile printing surface, it caused operational issues that were discovered while the printer was running. The extreme weight atop the structure made the superstructure more prone to leaning when it was unbalanced. Even a slight bend in the frame would cause unacceptable performance issues with any printing components anchored to the housing. Future improvements in this area of the design will increase the accuracy of the printer as well as its lifetime once any bent components are replaced with sturdier parts.

2.1.2 Ultraviolet Applications

UV light serves two purposes in this printer. The first, as discussed above, is as a sterilizing agent that denatures DNA within living cells, killing them. UV radiation passes uninterrupted through air, but cannot penetrate metal or plastics of any substantial thickness[53]. For this reason, the cleaning program maneuvers the print head around the centrally-mounted UV light so that every part of the printer is cleaned. Ultraviolet wavelengths are also harmful when shone directly to human retinas, so care has been taken to ensure that the printer will only be cleaned when it is covered by a veil or when nearby personnel are wearing UV-blocking personal protective equipment[50]. At the same time, high-energy photons are useful as a chemical initiator because they carry enough energy to interact with physical structures[50].

Each UV photon is roughly twice as energetic as a red photon and can excite electrons into higher states, as they do with fluorophores, or cleave a chemical bond, as with photoinitiators[43]. The mechanism of these reactions is known as the photoelectric effect, famous for earning Albert Einstein his Nobel Prize in physics. Applying this energy in a targeted manner allows the user to precisely build structures whose mechanical properties are controlled by results of the photoelectric effect. Later in this paper, the use of near-ultraviolet laser light is discussed as a means of controlling the physical properties of printed silk hydrogels. Because the UV bulb is much more powerful than the basic laser used to treat the inks, it would be possible to use the light to harden riboflavin-based gels that do not need to include cells.

2.2 Electronic Controls

The board that controls the printer is a Geeetech GT2560 board specifically designed for this type of custom-built 3D printer. It includes ports for five stepper motor controllers that can run six motors semi-autonomously. Those motors control the x-axis, y-axis, and z-axis movement (along with an optional second z-axis motor that moves in tandem with the first) in addition to two extruder motors. The board is also capable of routing power to a heated build plate extruders, as well as cooling fans. Inputs for six end switches control the minimum and maximum displacements for the power screws. The GT2560 board interfaces directly with whatever chosen software the user wants using a USB type B port. If, instead of using an external user interface, the operator chooses to work directly with the board itself, there is a LCD screen terminal. Finally, a small red reset button allows the user to cancel all work in progress and flash the memory on the board in case of emergency.

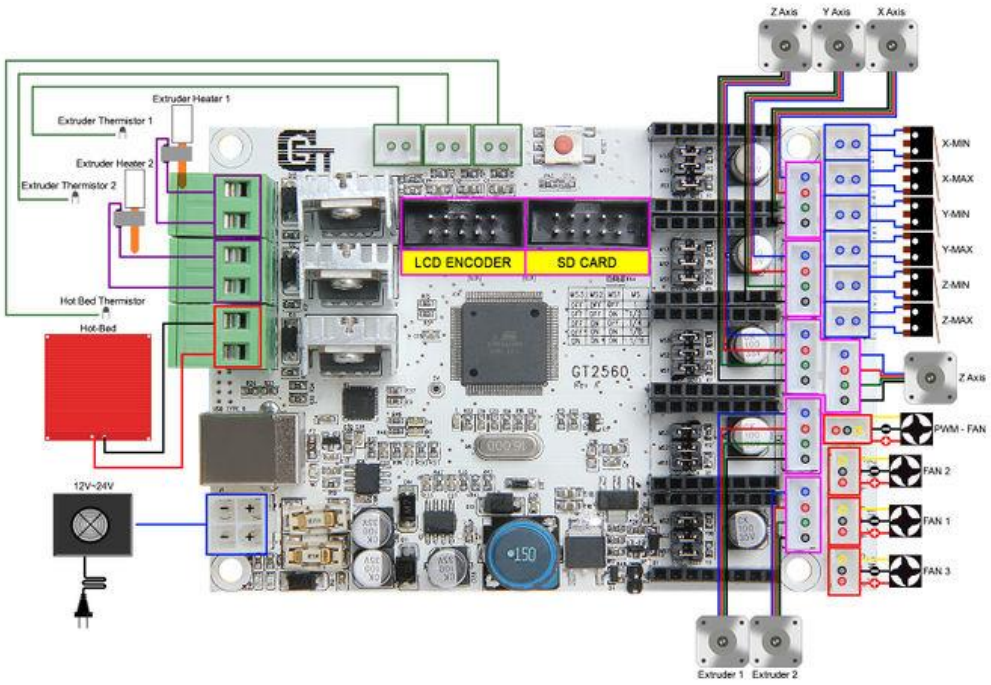

Figure 8: Wiring schematic of a GT2560 board displaying the different ports on the board. Image source: Geeetech.com

2.3 Software

Since 3D printing broke into the consumer market in the mid-2000's, more than a dozen different companies have built their own custom software for 3D printing. The most common category of software is a slicing program, a tool that takes the solid shape and creates stacked linear toolpaths for the print head. Those solid shapes are usually stored in STL (STereoLithography) files[34], a file type invented in the 1980's by the very same 3D Systems Company that pioneered stereolithographic printing. STLs work by tessellating a pattern into a solid shape defined by fused triangles[25]. Each company's software exists to occupy a single niche of this growing market, and there are even products whose sole purpose is to check if an STL model made with a different program will be compatible with a third party's hardware.

Cura is a widely-known open-source software package that gives the user broad control over a 3D print job. It was briefly used in the Omenetto lab because it was capable of manipulating both the solid CAD model and the finer controls of the printer itself. Since then, research has moved to Repetier-Host, a more powerful 3D printing software that provides unprecedented control over the actions of the printer at the expense of intuitive controls. Specifically, users in Repetier-Host can edit the "G Code" of the printer, or the actual machine instructions that are fed into the printer computer from the software. Line-by-line animations also display for the designer how the print head will move through the structure as it moves around the model, deposits support material, and builds the structure itself. Because the slicing program controls, G-code, and printer settings are all controlled by the user, there is a steep learning curve that makes interacting with the printer through Repetier-Host

more difficult than Cura. However, it was unanimously decided that having more power to control the exact motions of the printer was more useful than being able to start quickly. Below is the example startup page from Repetier-Host that shows some of the possible actions users can use to edit their print.

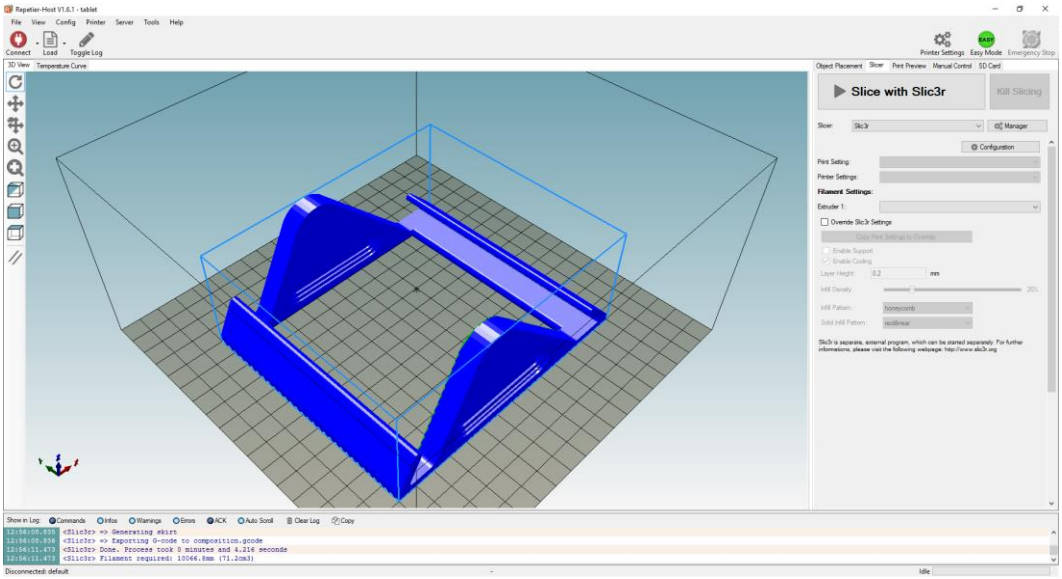

Figure 9: The start-up page for Repetier-Host showing user options (right) and an example print (left, blue).

In figure 9, on the right, note that this one screen shows settings for this specific print, for the printer, for the filament(s) used to build the structure, for the slicing program, and for the infill. No other freely available software covers this dynamic range of settings.

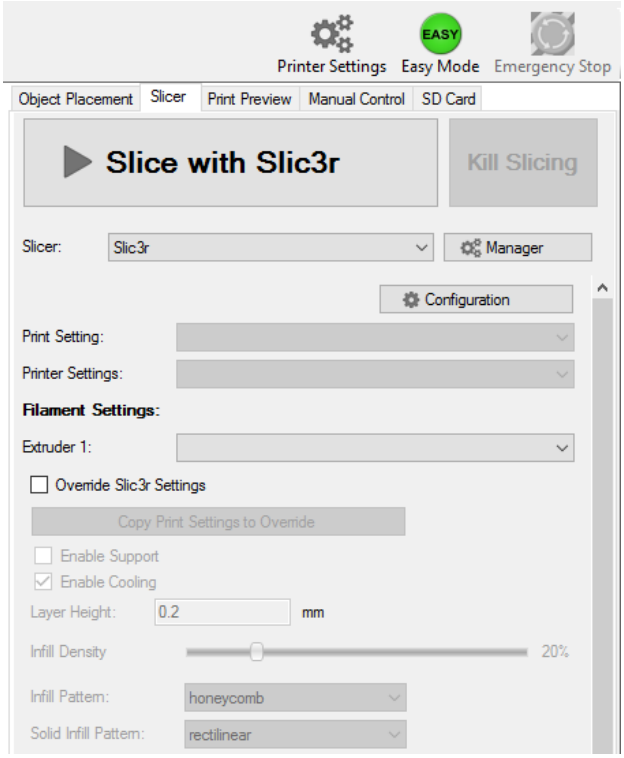

Figure 10: A close-up of the settings from figure 8.

Chapter 3 – Printable Biomaterials

3.1 Earlier Gels

For more than a decade, silk-based hydrogels have been studied by the Kaplan lab at Tufts University[41]. Early forms of the gels were cast in pre-made geometries in available containers and took weeks or months to gel[42]. Soon after, a much faster version of producing hydrogels was invented using aqueous silk that could gel within five days[15]. More recently, research has focused on making the properties of the gels controllable and otherwise increasing the options for customization[60]. Stiffness, degradability, immune response, and printability have all been targets of formula optimization[64].

Within the Omenetto lab, researchers have focused on gelling the inks as quickly as possible, often at the expense of the final toughness of the gel. Thankfully, the variety of mechanical properties exhibited within human tissue allows each of these structures to serve a unique purpose even with its lowered toughness[19]. In fact, because these gels can be made more quickly and without harsh chemicals, they fulfill their niche better than some stiffer gels that take longer to form[82]. To understand the scale of this difference, previous gels had reported compression moduli in the megapascal range[15], while silk-gelatin-glycerol gels were formed with moduli in the hundreds of Pascals. For reference, consumer plastics could have elastic moduli in the megapascal range, but the vast majority of human tissue has an elastic modulus below 20kPa[19]. With that in mind, one primary goal of this work was to create gels that could be made quickly as the silk-gelatin-glycerol gels but with a stiffness closer to physiologically relevant levels.

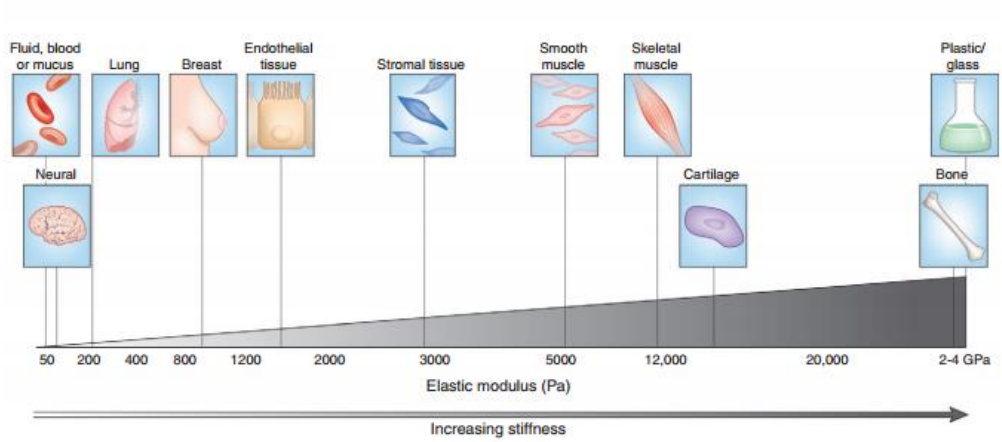

Figure 11: A comparison of the elastic moduli from different sections of tissue. Image source: (Cox, 2011)

What constitutes a physiologically relevant stiffness depends entirely on the purpose of the gel. If the purpose is to mimic the extracellular matrix of human tissue *in vitro*, then the values from figure 10, above, are a valuable approximation. It has been shown that depositing cells on a surface whose physical properties mimic native tissue can drive differentiation[19]. If the hydrogel is going to be implanted in the body, it needs to be stiff enough to survive the attachment process, whether that means building in sutures to the edges of the implant or strong holds for bone screws.

As a final note, the next generation of silk hydrogels should strive to match the previous generation's biocompatibility with human mesenchymal stem cells (HMSCs), cells that are commonly used in human tissue scaffolds. Not only must the ingredients of the hydrogel be biocompatible, but the necessary processing steps must not cause uncontrolled cell death. Silk and gelatin are proven biocompatible scaffold materials[8,60], but the concentrations of riboflavin and glycerol during processing are important. If all 2mM riboflavin in the hydrogel were converted to 2mM oxygen radicals, that could be a lethal dose. Similarly, the 50% glycerol bath is hypertonic compared to the cells, causing dehydration and peripheral cell death.

3.2 UV Curable Inks

3.2.1 Mechanism of Light Curing

The most visible example of using light to cure photopolymers takes place in the dentist's office[47]. Since the 1970's, restorative dentistry has utilized ultraviolet and blue light to rapidly and efficiently activate photoinitiators such as camphorquinone[4]. Photoinitiators can be sorted into two categories: those that release free radicals upon irradiation and those that can catalyze the creation of free radicals while in their excited state. Simply speaking, category I photoinitiators are light-sensitive reagents[28] while category II photoinitiators are light-dependent catalysts that rely on the presence of a co-initiator[67]. Pure riboflavin is a category II photoinitiator commonly paired with an amine molecule used as an electron donor[26]. The aromatic rings visible in the image on the right are hallmarks of a light-absorbing chemical[4]. In cases where the biocompatibility of the hydrogel precursors is paramount, naturally occurring amino acids like L-arginine can be used to ensure compatibility and solubility[40]. The image to the left exemplifies how L-arginine can serve as an electron donor in the same fashion as other amines.

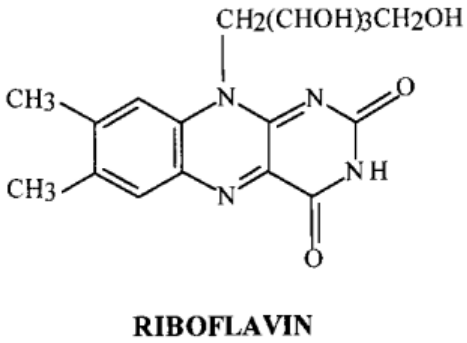

Figure 12 A Riboflavin molecule. Image source: Encinas, et. al. (2001)

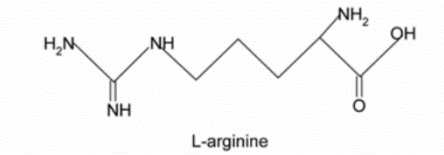

Figure 13: L-arginine amino acid. Note the two amine groups that serve as electron donors. Image Source: Kim, et. al. (2009)

In this project, the salt conjugate form of riboflavin used was not pure riboflavin but riboflavin 5'-monophosphate sodium salt hydrate. The addition of the hydrated sodium-phosphate group makes this molecule a category I photoinitiator capable of cleaving the phosphate group from the parent molecule under UVA or blue irradiation.

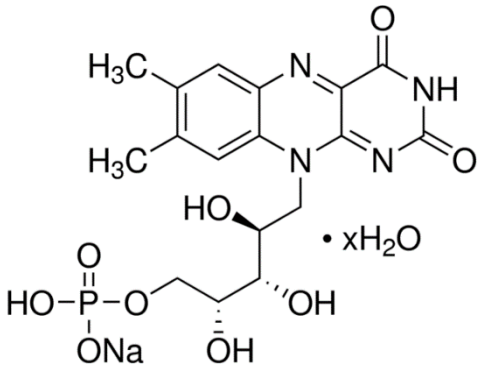

Figure 14: Riboflavin 5'-monophosphate sodium salt hydrate. The orientation is inverted relative to figure 3. Image Source: Millipore Sigma

Intuitively, the absorbance spectrum of this form of riboflavin matches that of pure riboflavin[45] including the UVA/UVB/blue light absorption[11,46] because the aromatic rings remain unchanged.

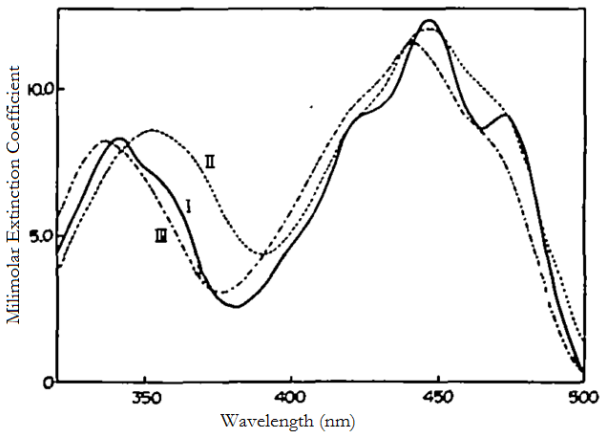

Figure 15: The absorbance spectra of riboflavin tetrabutyrate in three organic solvents, denoted with roman numerals[45].

As discussed later in this section, the riboflavin in this study is excited by blue (450nm) or violet (405nm) light either in a glycerol bath or in air. In organic solvents with neutral pH levels[24], riboflavin absorbs twice as much blue light as it does violet light[74].

While the solutions are still liquid, meaning that a scratch on their surface would disappear[2], they can be referred to as a printable ink or as an un-crosslinked solution. Once the mixture has solidified to the point where a superficial mark would become permanent, the ink has become a gel.

3.2.2 Ink Formulation Methods

The formulae used to create each gel were adapted from unpublished work done in the Kaplan and Omenetto labs by Mark Applegate and Maria Rodriguez. The principle components of the gels are silk fibroin, gelatin, glycerol, and the riboflavin salt that acts as the gelation agent. Using Rodriguez's work on the optimal process parameters as a starting point, riboflavin was introduced to increase the efficiency of the gelling process. Applegate's work details the process for creating gels solely from fibroin and riboflavin[8]. A summary of the gel formulae analyzed in this work is included in the next section. Regardless of the experimental treatment of the gels, the steps to produce the liquid ink remained the same. For convenience and understandability, the methods detailed below are written as step-by-step instructions. Unless stated otherwise, chemicals were obtained from Millipore Sigma (previously Sigma Aldrich).

To prepare gelatin for use in these inks, 175 bloom gelatin was dissolved to a concentration between 330-400mg/mL and stored at 60ºC. Higher molecular weight gelatin was found to be difficult to concentrate at that level and caused uncontrolled gelling in the ink. Similarly, glycerol was purchased at a purity of greater than 99.5% and diluted to 70% for use in the gels. Glycerol baths, when used, are 50% glycerol and 50% deionized water. Stock solutions of riboflavin are concentrated to 20mM or 40mM depending on the final volume requirements of the ink. Unlike the other components of these inks, silk solutions cannot be purchased in bulk and have to be prepared in the lab[63]. This lengthy process can be summarized as: dissolve silk fibers to isolate the fibroin and dialyze the resulting fibroin/salt solution to create a pure fibroin/water mixture at roughly 5%. Concentrate the fibroin to at least 20% but no

more than 35%, where experience shows that the shear necessary to extract a volume of the silk solution causes partial gelation. Any future references to aqueous silk are describing this silk fibroin solution.

It is important that the ingredients for the inks are added quickly, though it is not necessary to attempt to add multiple ingredients at the same time. Because the end goal is to form a gel from this ink, both the timing of gelation and the homogeneity of the solution require that no more than 20 minutes should be taken to form one batch of inks.

Once all the other liquids are ready, a small volume of deionized water, usually less than 1mL per ink, should be set aside before mixing the ingredients. It is necessary to set the final volume of the gel before adding any ingredients. Additionally, take care not to create bubbles in the ink, or at least to remove them before the gelling process in the next paragraph.

First, preheat 25mL glass vials to 60ºC (140ºF) on a countertop hotplate. Cold vials can cause phase separation and premature gelation in the samples. Next, add pre-heated (at least 40ºC) gelatin solution until the final concentration will be 100mg/mL. It is not possible to use solid or powdered gelatin for this step. If the gelatin cools before it is added, reheat it to avoid forming a solid mass with a concentration gradient. As necessary, add the 70% glycerol so it will result in a 1-to-3 weight-to-weight ratio with the silk, but do not add silk until the end. Next, add any riboflavin so the final concentration will be 2mM. For example, if the stock solution is 20mM (9.57mg/mL for this particular riboflavin salt), use 10% of the final volume for the riboflavin solution. The second to last ingredient to add is pure water, which

is used as filler volume to reach the final volume minus the silk. Up until this point, ingredients have been added from most viscous to least viscous in an attempt to form as few bubbles and evaporate as little liquid as possible. Finally, add silk until the final concentration is 100mg/mL. An example formula is shown on the next page for a hypothetical 1mL gel using all optional ingredients. With the addition of silk, the ink has unnoticeably started to gel and needs to move through the rest of the process expeditiously. If the solution contains riboflavin, it must be kept in the dark to limit ambient lighting effects.

Example 1mL UV Curable Silk Ink						
	Silk	Glycerol	Gelatin	Riboflavin	Water	Total Volume
Volume Added	333µL	48µL	303µL	100µL	216µL	1mL
Stock Concentration	300mg/mL	700mg/mL	330mg/mL	20mM		

Table 4: Example formula for a 1mL ink using the components in the first row at the concentrations in the bottom row. All values rounded to the nearest whole integer.

Once the ink has been formulated, lightly agitate the solution or vortex it without creating any bubbles for five seconds. At this point, the instructions diverge based on the final use of the ink. Detailed methods for each use of the ink are included in subsequent paragraphs.

For Printing: Pour the solution into the back of a capped 10mL luer-lock syringe and replace the plunger. Switch out the cap for a printing needle and expel the excess air until the ink comes out of the needle. The ink can be kept warm and pourable at 50ºC (120ºF) for up to six hours. When the ink cools it becomes too viscous to extrude, but as long as it does not gel it can be melted and reused within a day. Different printers may have slightly different printing protocols than what is listed here, but they must be capable of maintaining the ink at 50ºC.

For casting: Pour the ink into a mold at room temperature and agitate for an hour. This ensures the mixture will stay homogenous as it solidifies. After one hour, cool the ink to 4ºC (40ºF) for at least 6 hours but not more than 24 hours. This cooling period irreversibly solidifies the inks but does not crosslink them, at which point they will become gels. The ratio between the expected final volume of the solution and the volume of crosslinked gel was roughly two thirds, for a yield of 66%.

After the ink has been printed or cast, it can be crosslinked into a gel with light, a glycerol bath, or a combination of both. The methods for each type of crosslinking remain the same for both printed and cast gels. Laser-exposed gels were illuminated with a 12mW laser pointer with an emission peak at 405nm (violet light). Where blue light was used, three 450nm blue LEDs illuminated the samples from a distance of roughly 10cm (Appendix A) with a measured power output of 22mW at that distance. As noted earlier, the absorbance of riboflavin is generally higher in blue light (450nm) and ultraviolet light (350nm) than it is in the intermediate violet range. With that in mind, the blue LEDs likely excited riboflavin at a rate four times faster than the violet laser did, all other factors being equal. Future experiments could isolate and control for any discrepancies between the power output and absorbance rates in order to establish a relationship between energy and reactivity.

3.2.3 Experimental Gel Conditions

In order to understand the relationship between the compositions of the ink gels, their experimental conditions, and their final physical properties, dozens of gels were prepared and exposed to a variety of chemical and physical treatments. A

summary of those experimental conditions follows a brief description of each condition.

The first category of gels, those that served as the controls, were formed with only aqueous fibroin, gelatin, and glycerol. These were meant to emulate the properties seen in Rodriguez's work and would be the basis of comparison for all other gels.

The second experimental condition was a hybrid of Applegate's silk-riboflavin formula and Rodriguez's silk-gelatin-glycerol formula. In order to isolate the effects of the photoinitiator on the mechanical properties of the gel, these inks were exposed to UV light but were not crosslinked in a glycerol bath like the first group.

The third and fourth experimental conditions were the main target of this study. Both had riboflavin and glycerol in their inks, and both were crosslinked in a glycerol gel. Importantly, inks in the third experimental condition were not exposed to blue light, while those in the fourth group were exposed for the first 60 minutes of the glycerol bath. Further information about this method of light exposure is included in Appendix A.

The fifth group was an emulation of Applegate's formula that did not use glycerol either in the formula or to submerge the gels. The only method of crosslinking used on these gels was the 60 minute blue light exposure. Similarly, the sixth group did not have glycerol in the formula but was submerged in a 50% glycerol bath in order to identify any interactions between glycerol and the other ingredients in the ink. Finally, the seventh experimental condition was a minimalist formula containing only silk and gelatin submerged in a glycerol bath.

		Example Experimental Formulae						
		Silk	Gelatin	Glycerol	Riboflavin	Water	Light Exposure	Glycerol Bath
Experimental Condition	1	1.45mL	0.882mL	0.143mL	Ø	0.525mL	No	Yes
	2	1.45mL	0.882mL	0.143mL	0.300mL	0.225mL	Yes	No
	3	1.45mL	0.882mL	0.143mL	0.300mL	0.225mL	No	Yes
	4	1.45mL	0.882mL	0.143mL	0.300mL	0.225mL	Yes	Yes
	5	1.45mL	0.882mL	Ø	0.300mL	0.368mL	Yes	No
	6	1.45mL	0.882mL	Ø	0.300mL	0.368mL	Yes	Yes
	7	1.45mL	0.882mL	Ø	Ø	0.668mL	No	Yes
Stock Concentration		207 mg/mL	340 mg/mL	700 mg/mL	9.57 mg/mL			

Table 5: The seven experimental conditions studied as possible formulae for silk hydrogels. Formula 1 is the control, the other six are novel possible replacements.

3.3 Print-time Stability

There are a number of factors that affect the overall printing speed of the scaffold and therefore, the necessary stability of the ink. The most obvious of these are the cross-sectional area and the height of the structure, but these are wholly controlled by the designer. Less-often considered parameters are the speed of the printer's motors, the settings of the software used to run the printing program, and drying time in between layers. All of these have a direct effect on the amount of time that the ink has to spend sitting inside the print head, usually at a higher temperature, so it does not gel in the shape of the syringe. Time- and temperature-sensitive cell lines would consequently not be viable in certain printed scaffolds that they would otherwise be perfect for. Part of the goal in designing this printing system was to create a process that could produce previously impossible print jobs: larger tissues with finer features and incorporated cell lines. As a result, all the inks studied in this research were formulated with printing stability and cell biocompatibility in mind.

The current generation of bioplotters within the Omenetto lab can print a $1cm^2$ square tower at a rate of approximately one hour per centimeter of height. Given that the height of a print job is traditionally its limiting factor, it can be expected that the ink needs to be printable for at least two hours. This categorically eliminates enzymatic gelling processes which are traditionally very fast[59]. Similarly, cells that cannot withstand raised temperatures for two hours would need a modified printing regimen to be viable.

As discussed in section *3.2.2 Ink Formulation Methods*, the inks are stable enough at cooler temperatures that they can be reheated within 48 hours and printed again. Importantly, riboflavin inks need to be cool and obscured from light if they are to be reheated after a day. Individual cells could not survive two days inside the ink regardless of temperature or light exposure, so care must be taken to ensure that cells are printed as quickly as possible after adding them. It is possible to increase the viability of the printed cells by printing them directly into a media bath, or possibly by including cell media in the formula, but that falls outside the scope of this research.

Some factors that also control stability but are not studied directly here include the age of the silk and gelatin solutions, their concentrations, and the purity of the ingredients. Silk solutions must be kept cool but not frozen in order to preserve the homogeneity of the solution, while gelatin must be kept hot for the exact same reason. However, all the stock solutions used in this paper eventually degrade, with lower purity samples degrading faster. All experiments conducted in this research used the same stock solutions within three days of age for comparative studies.

3.4 Viscosity

In addition to the requirement that the gels are stable enough for the amount of time it takes to print, they must be capable of extruding through the printer's nozzle without freely flowing through it. This results in a narrow range of acceptable viscosities for each nozzle or needle diameter. Further limiting this range is the fact that high shear forces, a side effect of applying high pressure to viscous fluids, can cause the ink to gel inside the needle and permanently clog it[79]. Even before those shear forces clog the needle, however, they can kill cells while they're being extruded. A fine balance between surface tension and viscosity allows these inks to be deposited in a liquid form that holds its shape while it's printed and still support the cells inside the structure. As mentioned in the preceding section, the extrusion rate needs to be high enough to print quickly, but not so high as to gel the ink.

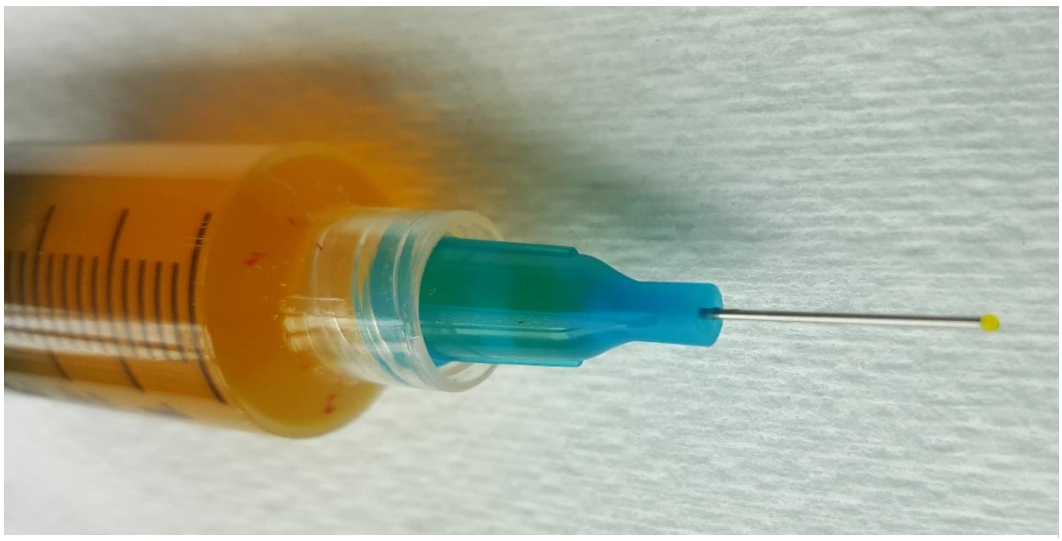

Figure 16: A drop of riboflavin-infused ink is extruded from a probe needle with an inner diameter of 300μm. For reference, a human body cell can have a diameter between 10 and 100μm[30].

3.5 Gel Characterizations

Important in the understanding of a hydrogel's usability is its elastic modulus[58]. Gels with higher moduli are firmer, and generally speaking can accommodate higher resolutions and aspect ratios because they hold their shape

under strain from an applied load like gravity[71]. Four different experiments were performed in order to establish the improved mechanical properties of light-exposed gels to traditional silk hydrogels. In the first experiment, dynamic mechanical analysis was used to compare the compressive modulus of exposed and unexposed gels. In the second, single hydrogel filaments were stretched to failure to question an increase in the elastic modulus. Next, atomic force microscopy showed the accuracy and magnitude of the gelling effect that focused laser light could have on the hydrogels. Finally, the actual compressive modulus of the ink is compared with and without light by printing structures under the illumination of a laser.

3.5.1 Compressive Strength

In order to characterize the physical properties of these gels, six 3mL hydrogels of each formulae 1-7 were created. Four 8mm cylindrical biopsies were taken from each 35mm x 2mm gel and stabilized in phosphate buffer solution. Adapting the procedure outlined in *Partlow et al, 2014*, the 24 samples from each condition were tested in a TA Instruments RSA3 Dynamic Mechanical Analyzer (TA Instruments, New Castle, DE). Briefly, each gel was pre-cycled to at least 10% strain six times, if possible. The tangent of the stress-strain curve on the fifth cycle was taken as the compressive modulus of the hydrogel[59]. Not only is this procedure in line with *Partlow et al*'s work, it was shown to be an accurate representation of the elastic modulus from three additional tests reported in section *3.6 Discussion*. First, one test biopsy was cycled 12 times to demonstrate the variability from cycle to cycle for one gel. Second, eight biopsies were cycled eight times to show that there was no relation between the magnitude and the variability of the modulus measurement.

Finally, one biopsy from each gel of each condition was compressed to failure to ensure that the recorded compressive moduli were taken from the elastic deformation region. All values are reported as mean ± standard deviation. Values are taken to be statistically significant if the p-value from a 2-sample T-Test is less than 0.001.

Figure 17: Gels from Experimental Condition 1. These gels are the primary control group and are a copy of Maria Rodriguez's original formula.

Gels from experimental condition 1, pictured above, were made following Maria Rodriguez's formula for silk-gelatin-glycerol hydrogels. They do not contain riboflavin and are gelled solely by immersing the ink in a 50% glycerol solution until they opacify. While silk films are commonly formed in methanol, the organic solvent of choice for hydrogels is a 50% glycerol solution, which requires roughly 2.5 hours to completely gel the ink. The compressive modulus of the gels recorded from the fifth cycle was 4.97 ± 0.3kPa.

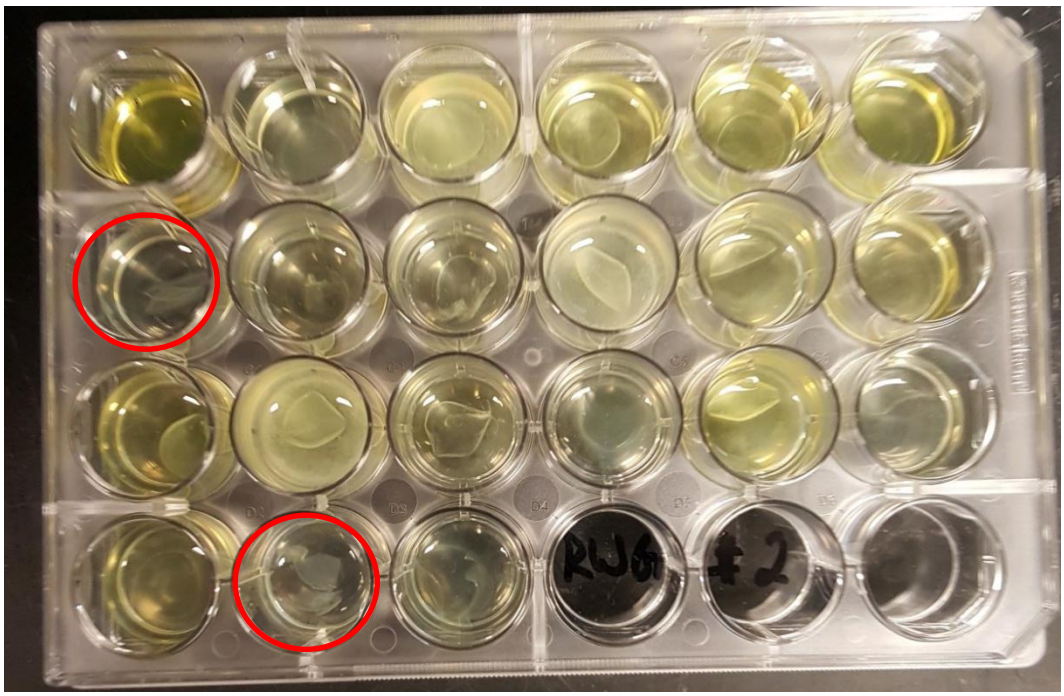

Figure 18: Gels from Experimental Condition 2. These gels were based on condition 1 but included riboflavin and substituted light exposure for the glycerol bath. Highlighted gels were torn by tweezers.

The second experimental formulation was similar to the first, but added 2mM riboflavin, the optimal concentration as investigated by Matthew Applegate. Instead of gelling these inks in an organic solvent, they were instead exposed to 763 Joules of light centered at 450nm by three blue LEDs (Appendix A). These gels existed to answer the question of whether blue light could be substituted for a glycerol bath without removing any other factors in Rodriguez's gels. Unfortunately, these gels could not support their own weight, as evidenced by the shredded remains visible in the highlighted wells in the picture above. Because they could not be gripped by tweezers, there is no recorded modulus data for these gels. It can be assumed that their modulus would be below 100Pa. It is possible that more light would eventually strengthen these gels to the point of holding their own weight, but it does not appear that this would be more efficient than the current glycerol process. Presumably, the intensity or the duration of the procedure would make such a process unwieldy.

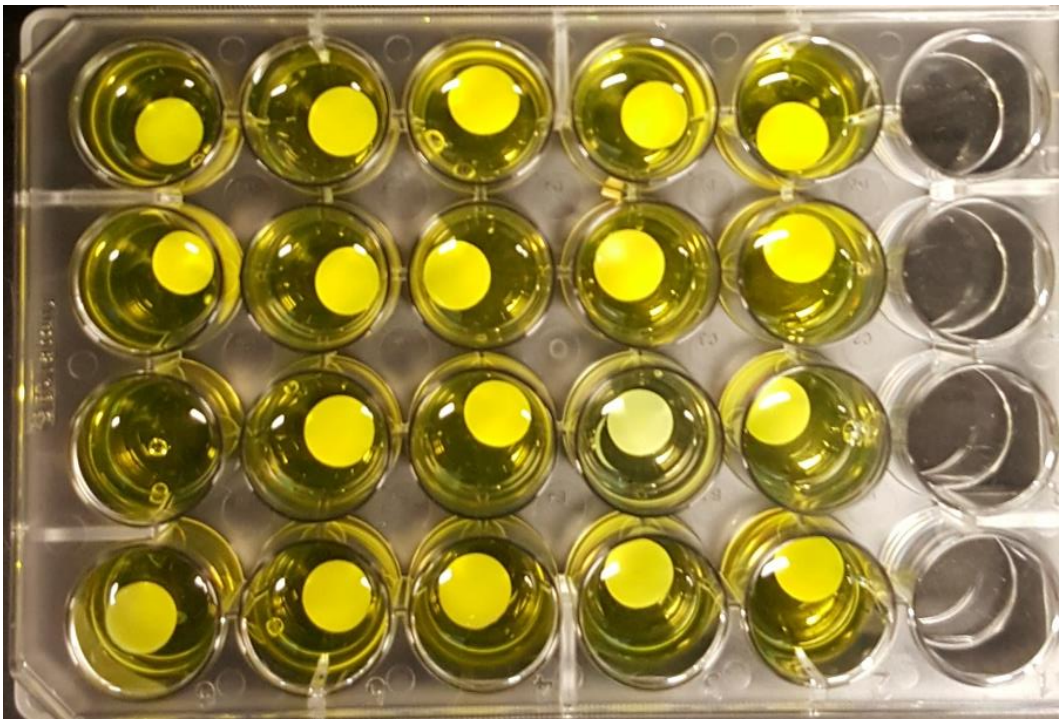

Figure 19: The third experimental condition used the same formula as the second, but was submerged in glycerol and obscured from ambient visible light. These gels served as the second major control group. Note: As previously mentioned, 24 samples were prepared from each condition though this photo shows a separate batch of 20 samples.

Experimental condition three also included 2mM riboflavin along with silk, gelatin, and glycerol, but was only treated with a glycerol bath. The yellow coloration of the gels comes from the natural absorption properties of riboflavin[4]. By keeping the ink covered with aluminum foil, it was possible to control for any possible reactivity caused by ambient lighting. This gel also served as a control for the fourth group by showing that the riboflavin on its own was not significantly increasing the stiffness of the gels. While Applegate demonstrated that light and riboflavin are needed together in order to crosslink silk gels, this group revealed that there was no interaction between the glycerol bath and the riboflavin that could have increased the efficiency of the crosslinking. The compressive modulus for this group was 4.91 ± 0.4kPa, as measured from the fifth cycle. As expected, this value does not differ significantly from experimental condition one ($p = 0.607$).

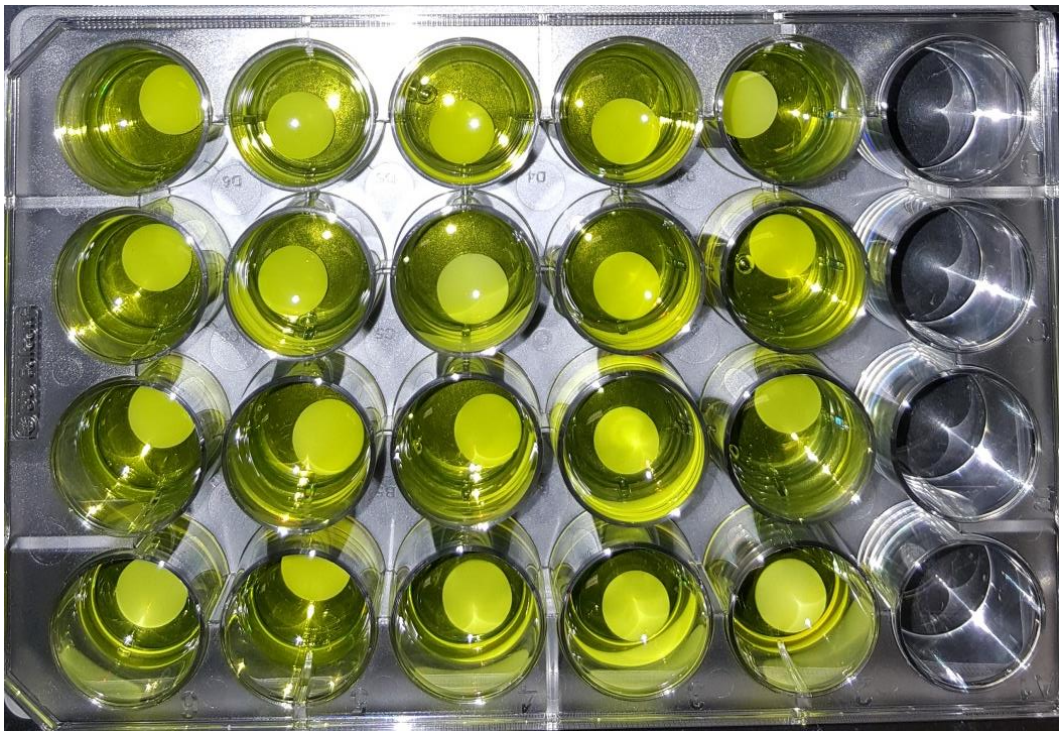

Figure 20: Gels from condition four were treated exactly the same as gels from condition three, but they were exposed to blue light for the first hour of the glycerol bath.

Condition four was the primary focus of investigation for this research. It included all the integral ingredients of condition 1 with the added riboflavin and light treatment expected to produce the best results. Briefly, as each ink was illuminated for the first hour (and flipped over at the half hour mark) as it gelled inside the glycerol bath. Between 75-90 minutes after the start of the glycerol bath, the gels visibly whiten and decrease the level of control over the amount of light reaching the sample[8]. Note that in the above photo the gels appear much whiter than the condition three gels due to the camera flash, but the gels truly are qualitatively brighter after exposure. This is likely due to an increase in crystallization within the gels, which is responsible for their characteristic white color. The measured compressive modulus for these gels was 7.49 ± 2.1kPa, significantly higher than both the condition 1 and condition 3 gels. The reason for this higher variance is the low amount of strain, which is discussed in section 3.6.

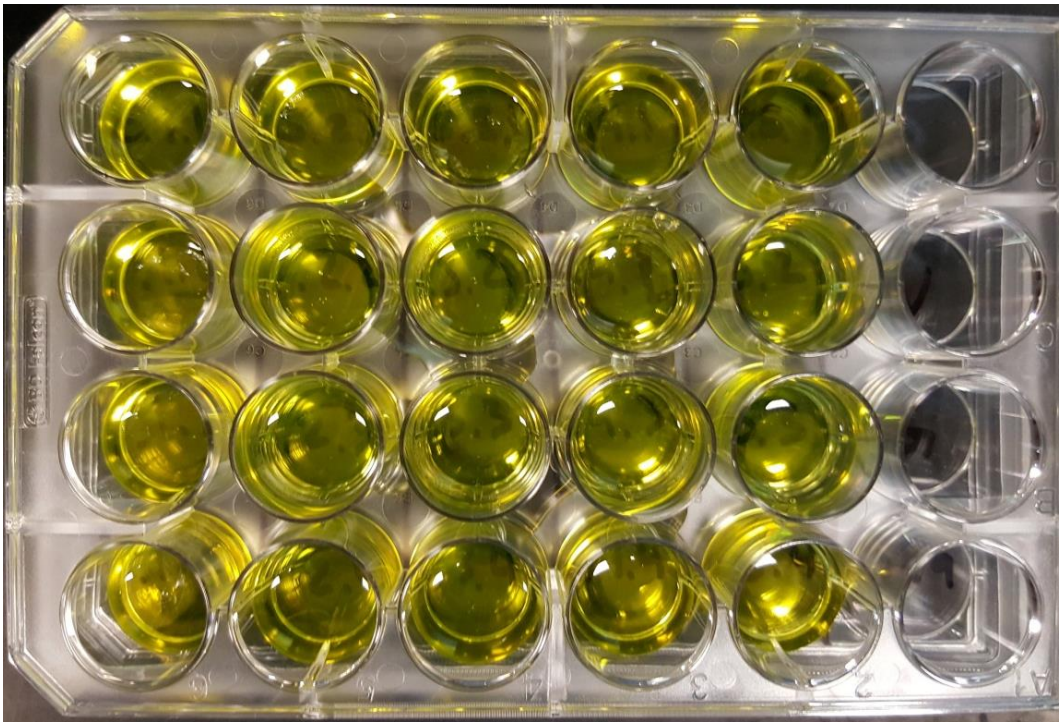

Figure 21: Condition 5 gels were made without glycerol and without submerging the ink in a glycerol bath. Similar to condition two, these gels were too weak to load into the DMA.

Condition five was created as an accompanying experiment to condition two, which studied the effect of using blue light instead of a glycerol bath to gel the samples. Unlike condition two, however, these gels also did not have glycerol within their structure. Both conditions ended up being too weak to load into the DMA and were cut up by the tweezers as soon as they were lifted from the PBS bath. No samples from this group were tested but it is reasonable to assume that their modulus would also be lower than 100Pa. Such low values approach the signal-to-noise limits of the DMA transducer, which measures the increasing force of the sample as it resists compression. If that force is too low, it is indistinguishable from the buoyancy effects caused by the compression plate lowering into the water bath and from ambient vibrations in the building.

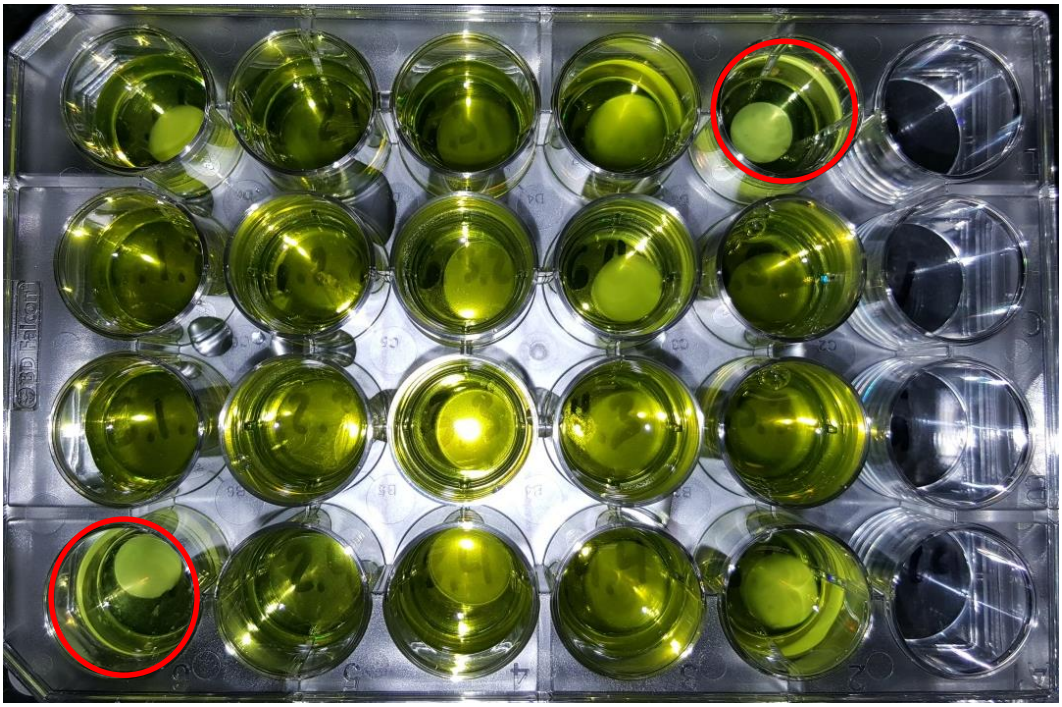

Figure 22: Condition six gels are translucent, unlike conditions two and five, because they were immersed in a glycerol bath that caused partial crystallization. Only the highlight biopsies could be loaded into the DMA.

Condition six was created to test whether the presence of glycerol within the ink formula was truly necessary to printing a robust gel. Other than the lack of glycerol within the formula, it was treated exactly the same as condition four. As the results show, glycerol is a vital ingredient in the composition of these hydrogels, as only two of these gels, the ones outlined in red above, could even be gripped with tweezers and tested within the DMA. Even still, the measured moduli were lower than 100Pa, barely registering above other sources of machine noise. Those two gels, visible above as the bottom-left and top-right, are visibly distinguishable as the whitest two gels, exhibiting their higher degree of silk crystallization. The reason for the variability in the stiffness of otherwise identical gels is not investigated in this report, but is likely due to phase separation within the ink.

Figure 23: Gels from condition seven are almost invisible because they contain no riboflavin, which provides the yellow coloration in other samples, and no glycerol, so the silk does not crosslink. Only the one highlighted biopsy survived to be tested.

The final experimental condition was created as a test of a minimalist hydrogel formula. Condition seven contained only a silk/gelatin mixture that was crosslinked in a glycerol bath, which is why the samples appear almost invisible in PBS. The top-right biopsy was the only sample that could be loaded into the DMA and recorded a modulus of just over 200Pa. For reference, gelatin hydrogels investigated elsewhere have reported moduli of elasticity in the 2-15kPa range[1], while a modulus of only 200Pa is near the lower limit for solids and is characteristic of a soft foam. It is not apparent in the image above, but even the cloudiest of the other biopsies tore under its own weight while being held with tweezers. As was the case with condition six, the cause of this outlier is unknown but could be the result of phase separation or uncontrolled variability in the glycerol bath.

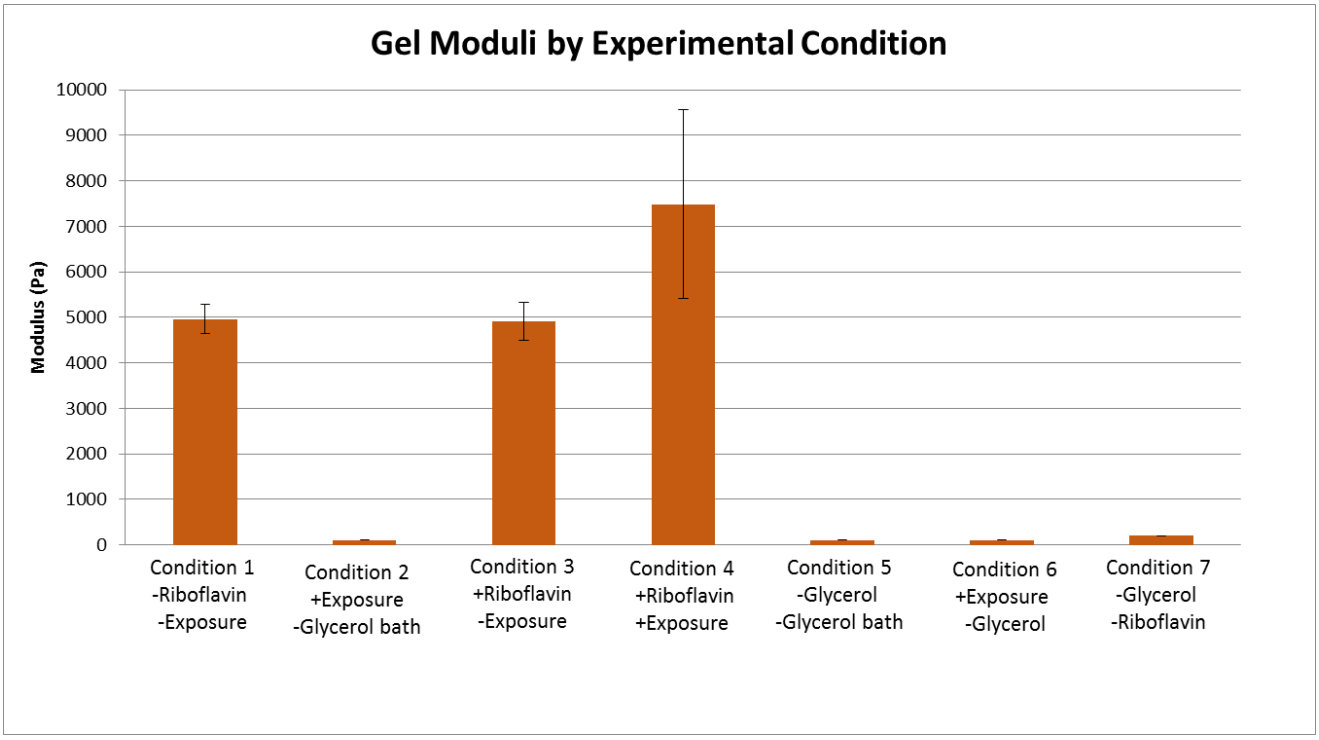

Figure 24: A summary of the elastic moduli of the gels as found from the fifth cycle. Error bars are one standard deviation. For a full list of experimental condition parameters, see section 3.2.3 "Experimental Gel Conditions."

The table above is a reduced summary of the compressive modulus of the gels as a result of their experimental condition. Note that all the exposed gels included riboflavin except condition 3, the second control. It is conceivable that the moduli for conditions 2, 5, 6, and 7 are higher than reported due to measurement errors and the length of time those samples spent in PBS, but they are expected to be an order of magnitude below conditions 1, 3, and 4. *Partlow et al* briefly investigated the correlation between the amount of time silk hydrogels spent in salt buffers and their measured stiffness[59], but this effect could not account for the differences between the experimental groups observed in the experiment above. Importantly, the work in this paper shows that removing any ingredient or process step from condition 4 would significantly weaken the structure of the gel. The most important step appears to be the 2.5 hour glycerol bath, without which the gels slowly disintegrate in PBS.

3.5.2 Tensile Strength

Building off of the compression testing, only two experimental conditions were tested under tensile loads. Fresh 3mL inks were made from condition one, the previous standard for silk-based hydrogels, and condition four, the proposed riboflavin-infused improvement. Following the procedure outlined above in the "*For Printing*" section, the inks were loaded into the bio printer and extruded into 2cm-long single strands, approximately 500μm in width. The riboflavin-infused gels were exposed with 405nm (violet) laser light that was focused on the strand and moved along its length as it was printed. All strands were chilled overnight to 4ºC and then gelled in glycerol for 2.5 hours. After the bath, the strands were imaged in order to establish their average width and then individually mounted in the DMA. The strands were pulled at a rate of 0.05mm/s until failure, at which point the elastic modulus was calculated from the elastic region of the stress/strain curve.

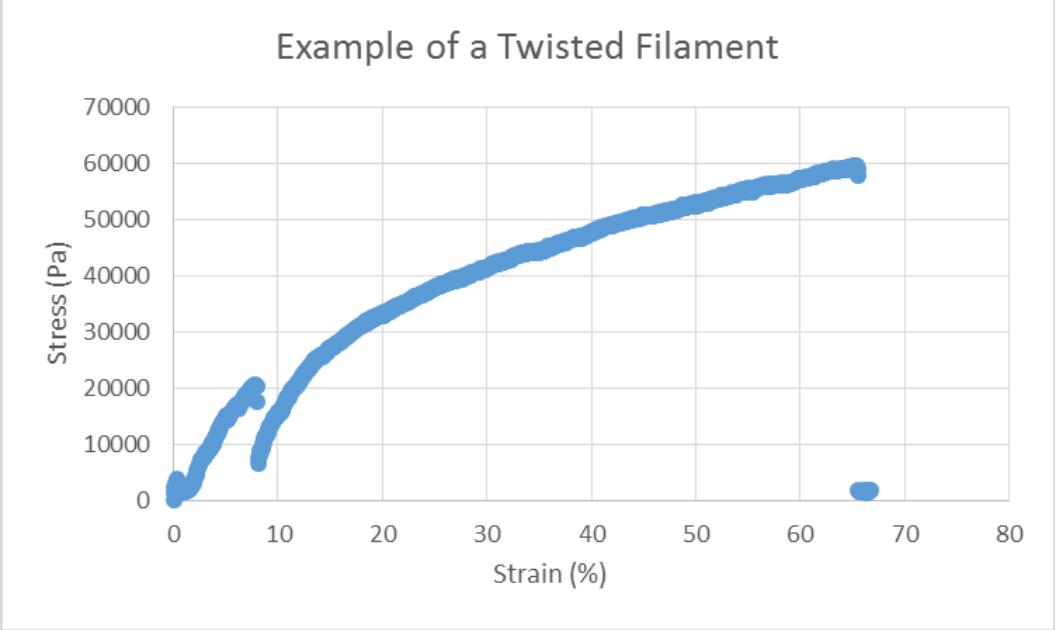

Figure 25: A stress/strain curve with a characteristic drop in stress at the moment the filament realigns.

As the figure above clearly demonstrates, deriving the young's modulus of a filament is not as always as easy as "taking the slope of the first linear region" of the stress-strain curve. That particular curve came from a twisted filament, which at first seemed weak, but then realigned and stiffened. Because filaments lose a significant portion of their strength for each twist in their length, samples like these have to be discarded. Ultimately, seven exposed and eight unexposed strands were successfully pull-tested in the DMA. However, before the tensile modulus can be measured, the "toe region" has to be accounted for, just as it was in the compression test[68]. Even perfectly flat and straight strands can have a toe region (see below) where the filament first appears to have a linear region of increasing stress, but is actually not being drawn taught. This results from the shape and composition of the filament. As the filament is drawn taught, the DMA can register slight fluctuations in the force needed to draw the filament straight, but only after the filament is aligned is it actually deforming elastically. This process is distinct from strain hardening, another aberration in the stress/strain curve, which is caused by the molecules of the filament itself slipping past one another into a stiffer, but deformed, arrangement. Soon after those molecular bonds slip and fail, the structure of the filament ruptures. The image on the next page illustrates a large toe region that has to be divided out of the actual length so that the stress/strain slope accurately describes the stiffness of the filament.

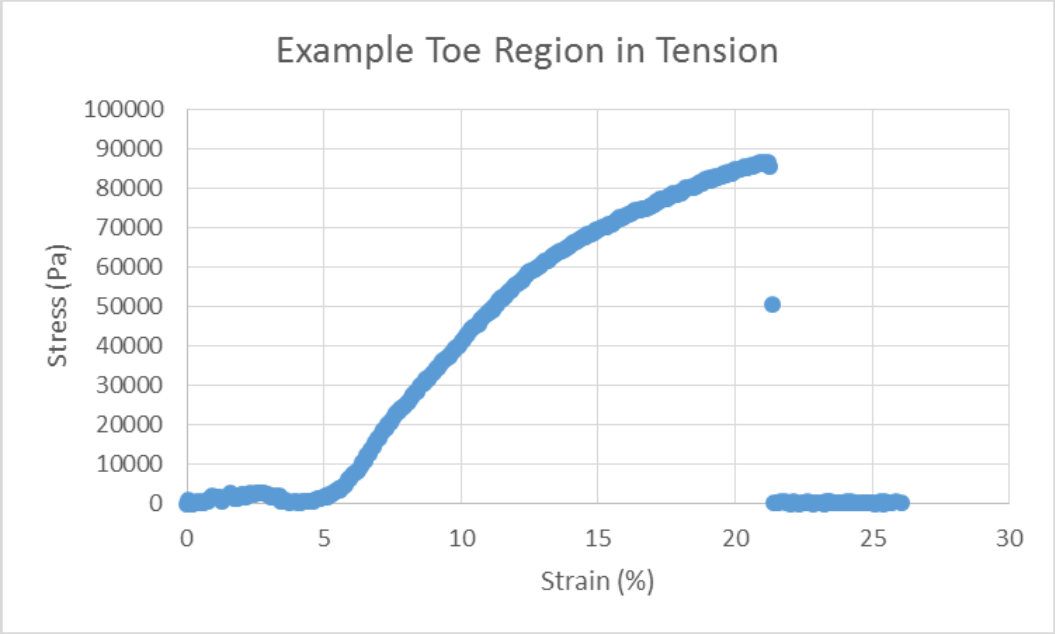

Figure 26: A stress/strain curve for a filament with a noticeable toe region (0-5% strain) that should not be mistaken for the elastic deformation region (6-10%). Notice the strain hardening from 15-20%, just before the ultimate strength and rupture.

At the end of this test, there was not a significant increase in the young's moduli of the condition four fibers compared to the condition one fibers. The exposed group had a young's modulus of 15.6 ± 6.4kPa while the unexposed group was just slightly lower, at 14.7 ± 2.0kPa ($p = 0.28$). It is important to note that are several factors that could mask any positive effects from the laser exposure. First and foremost, the amount of light delivered to the fibers was minimal. Aside from ambient light, the laser pass-over delivered roughly 10mJ of light, assuming that all the light was focused onto the strand and hit each point for just under one second. While the compression data showed that light definitely strengths these gels, a handheld laser was the lower bound for light exposure and was clearly insufficient to crosslink any silk during one printing pass. The printed towers, discussed in section 3.5.4, are a better example of the practical benefits of using unfocused laser light to build stronger structures. Additionally, single strands are susceptible to minute

contaminants that wouldn't affect the macroscale properties of cast cylinders or printed towers. The picture below makes clear not just that contaminants are of the same scale as the single lines, but that the line width can vary significantly along the length of the strand. One would expect the strands to fail (break) at their thinnest point, where stress pressures are highest, but it is impossible to know the weakest point in an uneven strand with invisible impurities throughout.

Figure 27: A microscopic photo of a single printed filament showing the variation in its width in one short segment and the presence of impurities.

For these reasons, this test proved to be more qualitative than quantitative, but showed no difference in the stiffness of the laser exposed strands nonetheless.

3.5.3 AFM Probing

Atomic force microscopes (AFM) are capable of directly measuring the mechanical properties at the surface of a material at the microscale[27]. While a microscope is used to observe the measurement, it is actually the deflection of an unseen laser light shined on a cantilever beam as it moves over a surface that records the mechanical properties. As the beam moves over the sample, it is depressed a few microns into the surface and the change in position of the laser as it reflects off the tip is correlated to the stiffness of the surface. Because the tip can be arbitrarily small, and the scanning area confined to less than $10\mu m^2$, precise regional differences in the stiffness of a surface can be recorded. The main drawback of using an AFM to measure these surfaces is that the scanning setup works best on harder, flat, and dry surfaces, but these gels are softer, contoured, and moist.

Riboflavin gel that was exposed to focused laser light for 60 seconds had cavities where the light indirectly cross-linked the silk. Because of these microscopic surface deformities, it was necessary to use an AFM to measure the stiffness around the focal point. Cantilever beams were specifically purchased for these gel measurements from Novascan (Ames, IA) with calibrated 20μm borosilicate glass beads beneath the heads of the cantilever. The larger beads reduced stiction between the beam and the gel, which otherwise would have made measurement impossible. The output from the AFM is processed through Yuqi Wang's proprietary MatLab scripts, though the outputs are shown below. Importantly, the z-axis is not the height of the sample, but its stiffness in Pascals. Unlike the compression tests, this data is for the surface of the sample only and does not account for the overall strength of the gel.

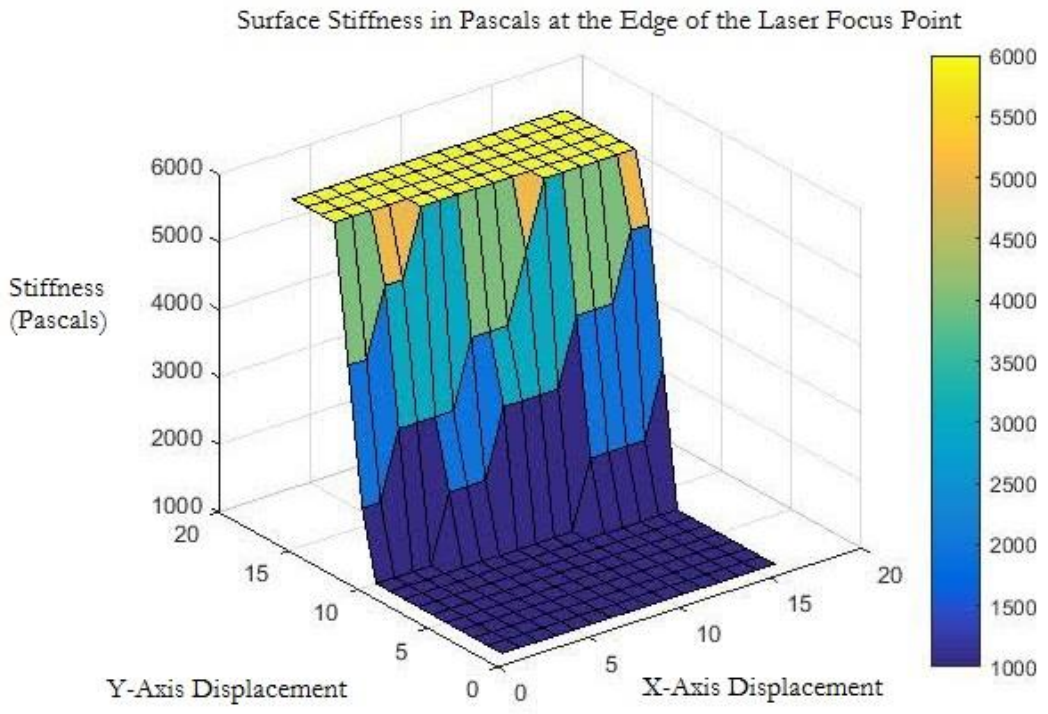

Figure 28: Surface stiffness of a laser-exposed gel as measured by AFM. The stiffness in Pascals is shown according to the color code on the right.

The data, taken from the edge of the laser focus point, shows a clear drop in stiffness only a few microns wide. This suggests that the free radicals formed as part of the photoinitiation process are highly concentrated within the area illuminated by the laser. The mean free path of reactive oxygen species within the sample is probably close to 3μm, though this would need to be confirmed with additional experimentation. Because reactive oxygen species can cause cell death[39], a short mean free path is good for cell- and tissue-biocompatibility. It is also remarkable how consistent the stiffness is within the illuminated area, where the surface stiffness is approximately five times higher than the surrounding gel. It would seem, then, that the laser light (totaling 1 Joule of energy) was evenly dispersed over the 100μm-diameter focal point.

3.5.4 Printable Tower Stiffness

Building stiffer molded structures is a noteworthy goal, but the stated desire for this work was to create a printing system capable of producing bigger, stronger structures. To that end, laser-exposed single filaments were studied in section *3.5.2 Tensile Strength*, but larger and stronger structures, as measured by elastic and plastic stiffness, are discussed in this section. The simplest possible test for an improvement in this area is to print identical towers, expose one group to light as it is printed, and compare the resultant stiffness of the structure. For this test, one large reservoir of ink from condition 4 was used to print all the towers. Exposed towers were illuminated by a laser beam aimed just below the extruder tip without a focusing lens. Keeping the beam pointed below the tip of the needle ensures the light contacts the structure as it printed without gelling the ink at the tip of the needle, which was found to cause clogging.

Given the print time of 20 minutes per tower, the output of the laser pointer (12mW), and the fraction of time the laser was over any point, it is estimated that each point received approximately five joules of light energy centered at 405nm. As with the compression data from section 3.5.1, 8mm biopsies were taken from the center of each tower after gelling the structures in glycerol for 150 minutes. Again following the procedure outlined in *Partlow et al*, The elastic moduli were calculated from the stress-strain data at 10-20% while the plastic deformation is measured from 40-50% strain[59].

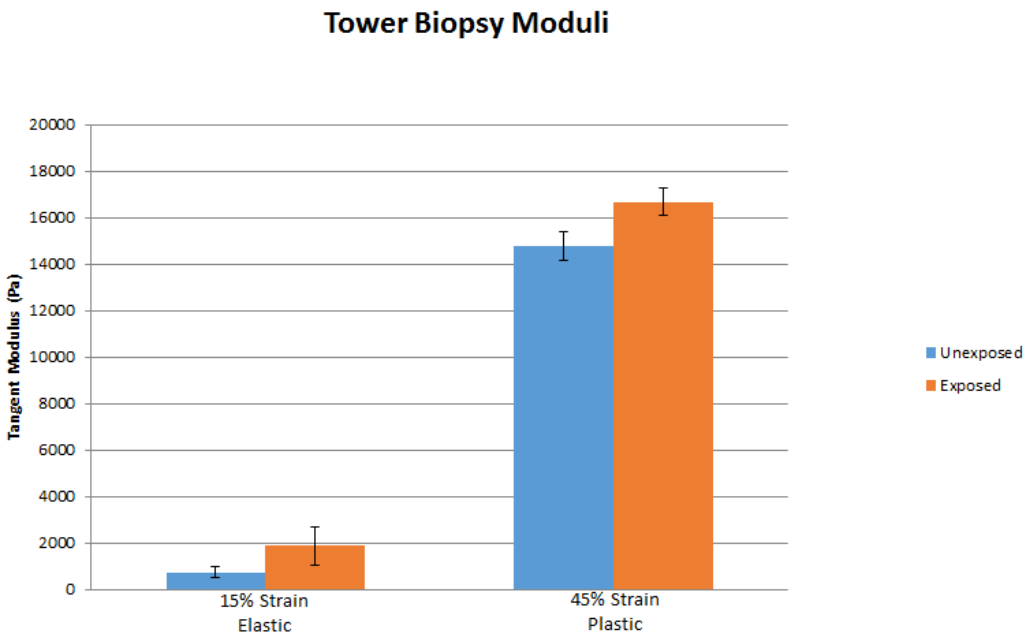

Figure 29: Modulus data for biopsies taken from the center of printed towers. Both groups were made from the same reservoir of ink, but the exposed towers were illuminated with 5J of violet laser light.

On average, the exposed towers had an elastic modulus (1,860 ± 825Pa) more than twice as high as the average unexposed tower (741 ± 208Pa). However, the magnitude of the standard deviation meant that the difference was statistically insignificant, even if the towers really were stiffer. Plastic levels of deformation were seen at strains above 25% in this test, but for consistency, all samples were measured at 40-50%. All the exposed gels were stiffer than all the unexposed gels, and they averaged 16.7 ± 0.6kPa vs. 14.8 ± 0.6kPa, respectively. According to a two-sample T-test, this difference was significant for $p < 0.01$ and makes intuitive sense. Combined with the data from sections 3.5.1 and 3.5.2, these values suggest that the 2mM riboflavin is saturated at light levels above 500J, unaffected by levels below 0.01J, and first significantly affected at around 5J. For more information about the upper limits of light levels and riboflavin saturation, see Appendix C, where timed illumination levels are compared against cyclic moduli.

3.6 Discussion

In section *3.5.1 Compressive Strength* the compressive modulus taken from the fifth cycle of each biopsy showed a significant difference between condition 4 and all other conditions, but curiously, this group also had a considerably higher standard deviation. The purpose of this section is to discuss why that result was found, what steps were taken to correct for it, and what conclusion the ancillary data supports.

The first step towards understanding the variability in the data was to chart the modulus of each biopsy in conditions 1, 3, and 4 grouped by the gel (one through six) it was taken from. That data, shown on the next page, demonstrated that most of the gels from conditions one and three had very little variation. Every single gel in those conditions yielded four biopsies with moduli within 750Pa of the mean. Only in the fourth condition did gels have biopsies with moduli approximately 7,000Pa apart from one another. The first observation that was made from this data is that no one gel provided all or even a majority of the abnormally low reported values. Second, because one gel had two relatively high moduli and two of the lowest, it must have been the case that the highest biopsy was immediately adjacent to at least one of the low outliers.

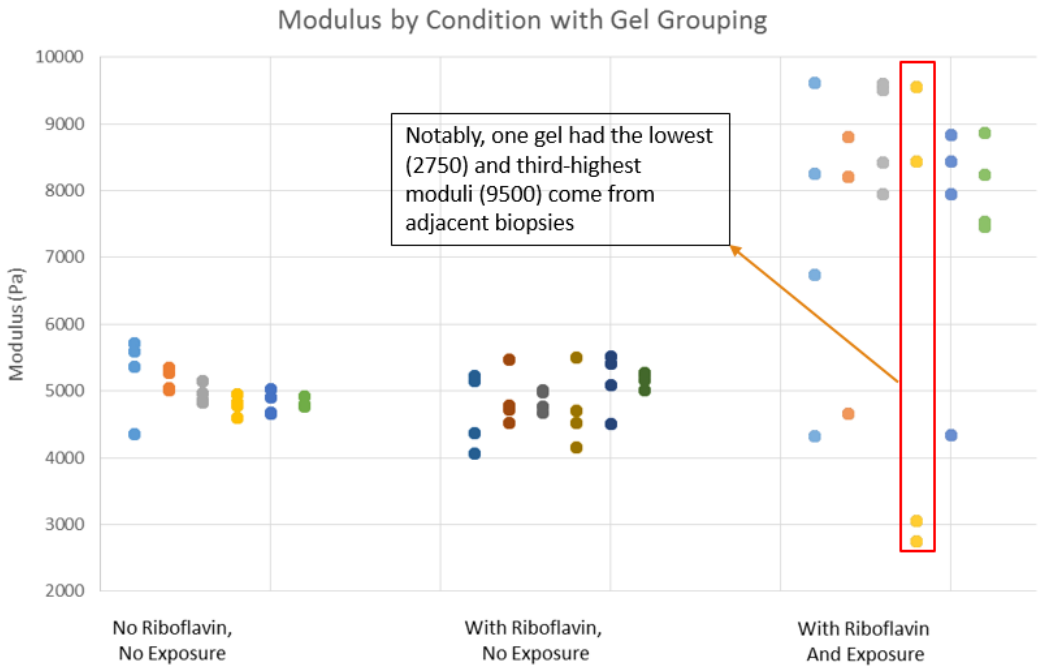

Figure 30: Compressive modulus data as measured from the line of best fit in the stress-strain curve from the fifth cyclic load.

As the picture below shows, it was also not the case that any of the biopsies from condition 4 were taken from an edge region, where the moduli might differ from the middle:

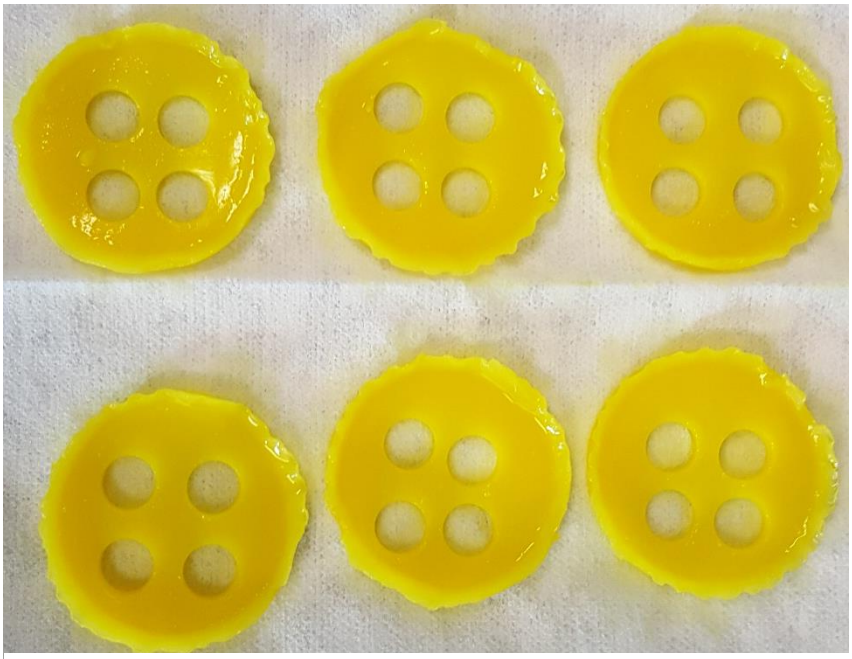

Figure 31: The gels from condition 4 showing 24 biopsy locations all well within the center of the gels. Biopsy diameters are 8mm, gel diameters are 35mm.

The next area of concern was that the fifth load cycle would be significantly different from those before and after it. The concern here is whether gels that were accidentally loaded one time too many or too few would record different results. The first test for this was to cycle one gel twice as much, meaning twelve times, and see if any cycle were greatly different from another.

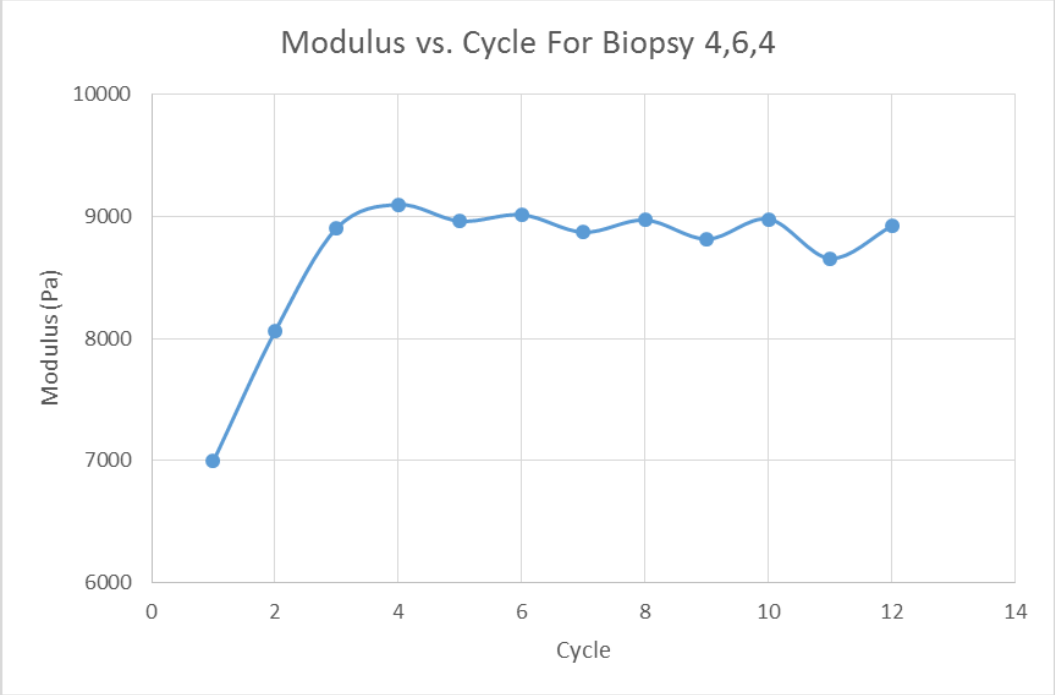

Figure 32: The measured moduli from 12 cycles of biopsy 4,6,4 (Condition 4, gel 6, biopsy 4).

The results reaffirmed what *Partlow* had written about preloading the gels[35] and did not support the idea that one cycle off from cycle five could account for the differences in recorded moduli. Indeed, the moduli from cycle 3-12 all fell within about 5% of each other, which could not explain the 200% increase from one biopsy to the other that was observed. As expected, this data supported the need to precondition the gels, and showed that cyclic loading did eventually take its toll on the strength of the gels. The odd numbered cycles, those started from rest, declined slightly after cycle 5, but the even cycles, those with no rest, showed less variation.

In order to investigate the possibility that some gels might show more variation from cycle to cycle, seven other biopsies were also run to cycle 8 and the moduli from each run were compared:

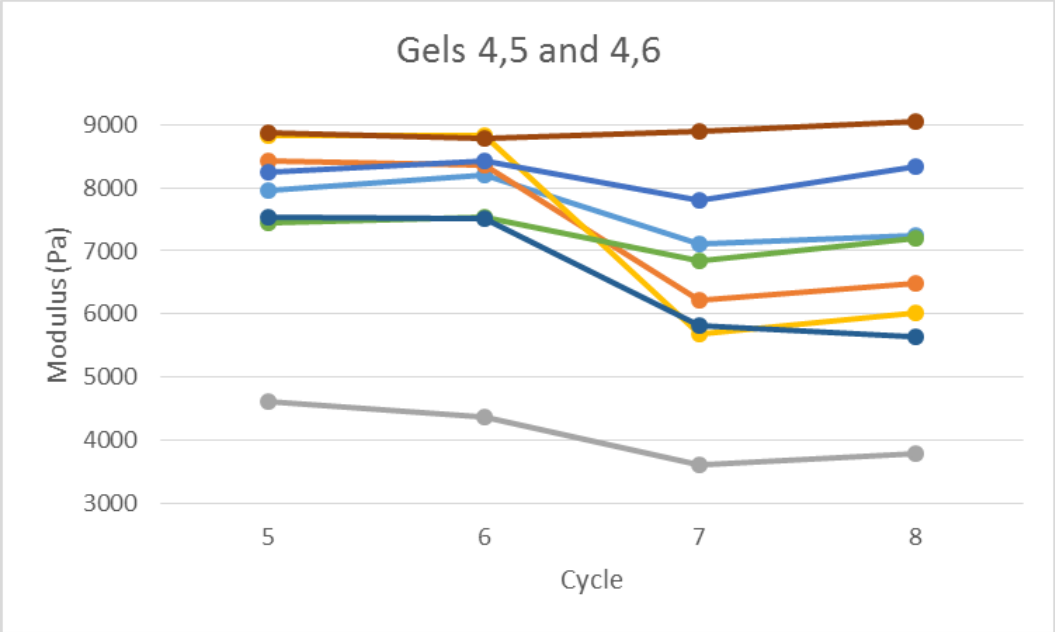

Figure 33: The moduli from eight biopsies (two gels) were recorded from cycles five through eight to see if some gels might display unusually high variability.

This test included one of the suspiciously low moduli biopsies but all this data showed was that the higher moduli stayed high and the low moduli stayed low. There was no crossover from one range to the other that could have explained why some biopsies seemed to be significantly weaker than their neighbors. It was also not the case that one gel had higher variability than the other. Gel 5 was on average weaker than gel 6, but this difference is not significant (the biopsies, not the gels, are color coded in this graph). This data is rearranged below to make it easy to see that the high values stayed high while the low values stayed low with no correlation between stiffness and variability.

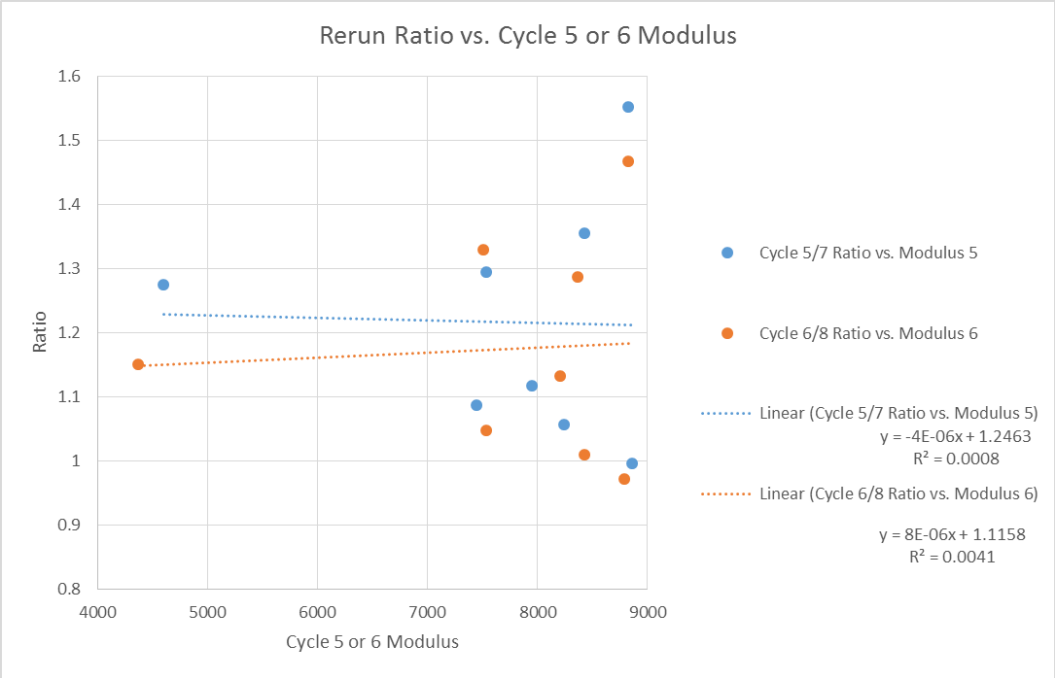

Figure 34: Shown here is the correlation between the stiffness of the biopsy (as measured by cycle 5 or 6 modulus) and how much that modulus changed in the next run (cycle 7 and 8).

It is most useful to compare the cycles from rest against one another and the rebounding cycles against one another because they represent similar conditions. The moduli from cycle 5 or 6 was divided by cycle 7 or 8, respectively, and graphed against the modulus from the lower cycle. For trend lines, R^2 values range from 0 to 1 and characterize the fit of the data to the trend. Values above 0.95 suggest a strong fit, while these values (0.0008 and 0.0041) suggest no trend at all[66]. There is no evidence that the weaker moduli were measured from a single weak cycle within a strong biopsy. It could only be the case that the DMA was not making full contact with the biopsy, which would cause the modulus to seem much lower. This could be caused by uneven surface topography, where the DMA senses the highest point of the gel, but never reaches the full flat surface within the 10-12% strain. One way to test for biopsies with uneven peaks would be to look for gels that are taller than their peers. Not all tall gels would be uneven, but uneven gels should be tall.

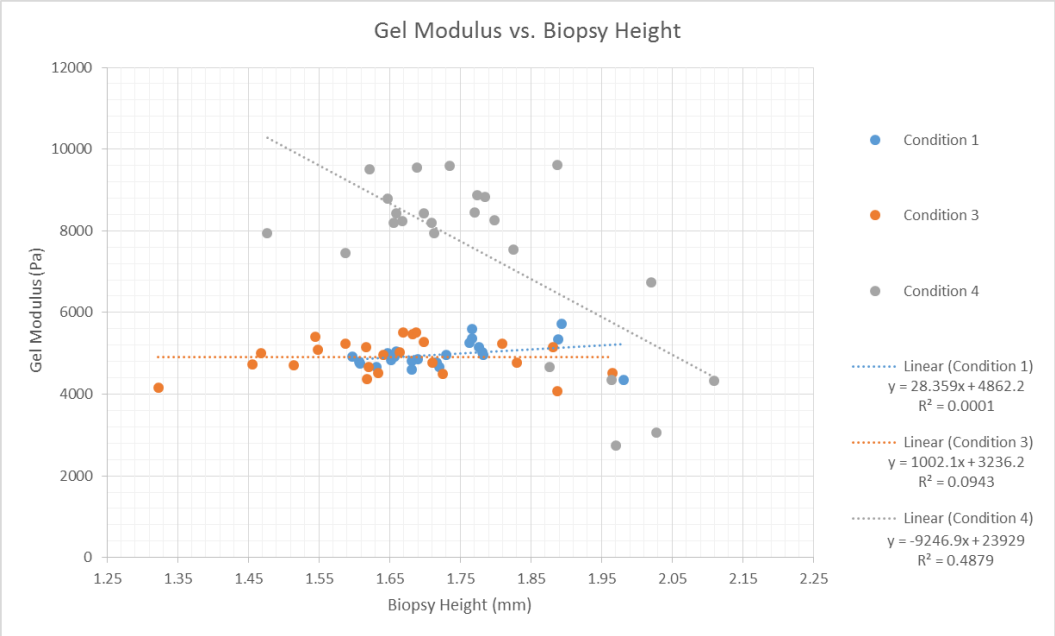

Figure 35: The relationship between the height of each biopsy and the measured modulus of the gel helped reveal that lower values were attributable to taller gels.

Just as predicted, all the weakest moduli were recorded from seven of the eight tallest biopsies. Unlike condition 4, conditions 1 and 3 showed almost no correlation between height and modulus, as expected from their lack of variation. This was proof enough that uneven surfaces indirectly caused low moduli readings to warrant a final DMA test of representative samples.

Six biopsies each from conditions 1, 3, and 4 were compressed to failure in the DMA to ensure that the linear elastic region was captured in the data. As the stress/strain curve on the next page exemplifies, the first 12% strain captures the very beginning of the linear region, but the toe region is close enough to potentially cause interference in a linear fit of the last 5%. For all 18 retested biopsies, linear fits from 15-25% strain were taken with R^2 values above 0.999, compared to values below 0.995 for the low cycle 5 moduli.

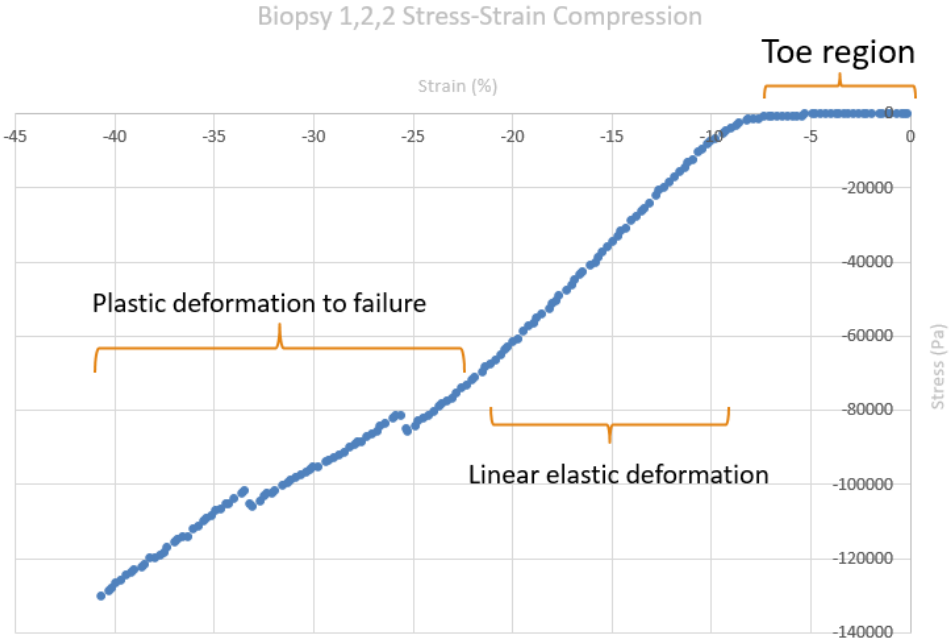

Figure 36: A stress/strain curve representative of an unexposed gel fracturing.

It was qualitatively observed in the failure testing of these gels that unexposed gels fractured, rather than crushed, as the exposed gels did. The elastic moduli were re-recorded from the biopsies, including some of the low outliers, and the variability disappeared from the data. Condition 4 is significantly stiffer than either other group, but is not now significantly different from the value reported in section 3.5.1.

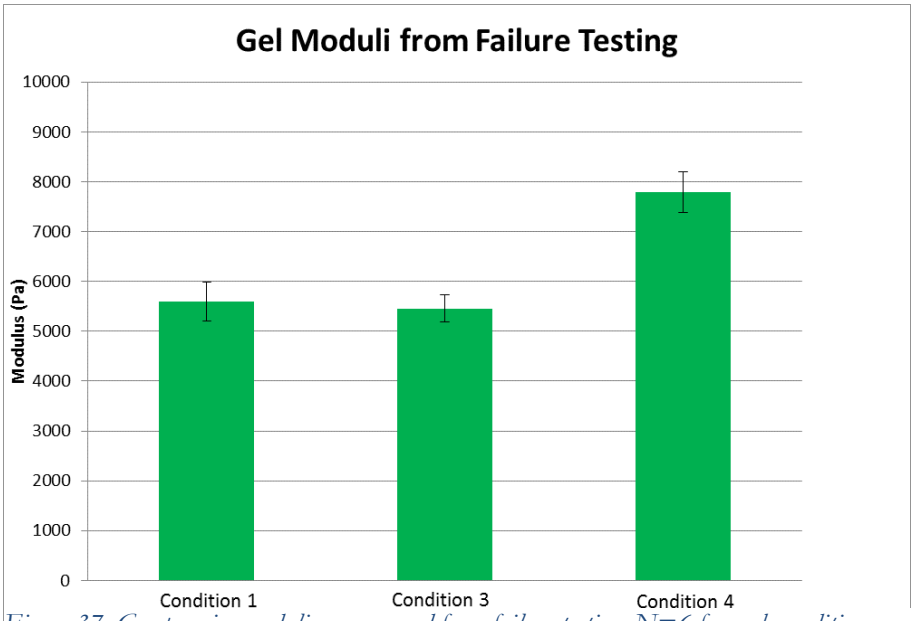

Figure 37: Compressive moduli as measured from failure testing. N=6 for each condition.

It has been reasonably established that the low outlier values are the result of beginning the compression measurement too high above the flat surface of the biopsy. To demonstrate this point, the charts below reveal how the "weakest" cycle 5 modulus was measured from a short linear region (left side), visible in the failure testing (right side) before the true elastic deformation began.

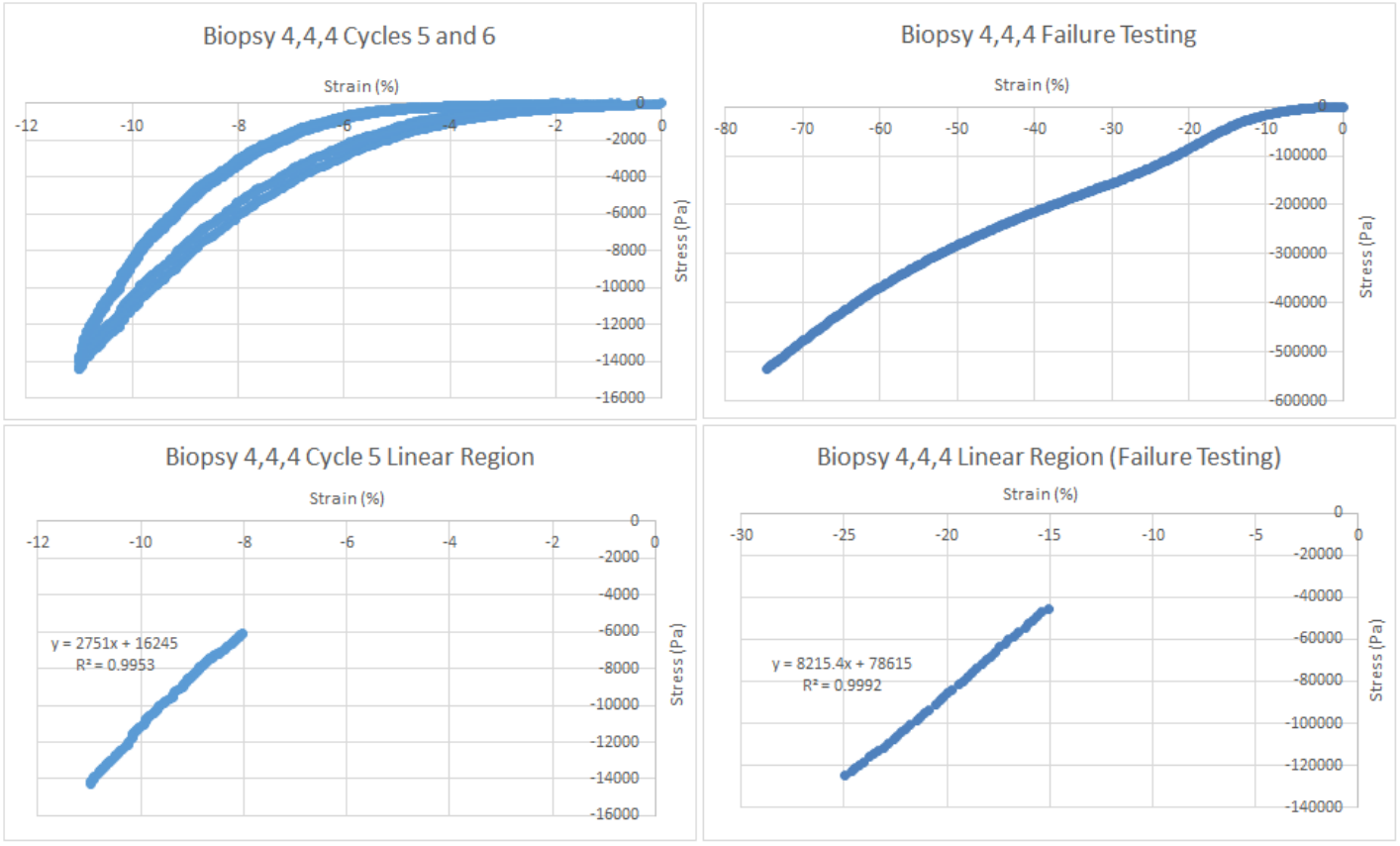

Figure 38: A side-by-side comparison of the cycle 5 and failure testing for one of the low outliers.

Even in the failure testing, the 8-11% strain would have yielded an abnormally low modulus of 3500 Pascals, though it is now obvious to see that this strain is within the toe region. Future researchers can avoid this pitfall by choosing a higher normal force as their start point or by compressing into strain values above 20% in cyclic loading.

Chapter 4 – Current Applications

4.1 3D Printed Tissue Replacements

While the field of tissue engineering has yet to print a functional, three dimensional organ from stem cells, there has been significant improvement in the field of tissue replacement[18]. In the last two years, limb prostheses have increasingly been 3D printed to keep costs down while improving availability[37]. Whereas traditionally manufactured leg and arm replacements can cost upwards of $100,000 3D printed alternatives can be made as cheaply as $50 with comparable usability.

Figure 39: A higher-end prosthetic made by 3D Systems to showcase the beauty and intricasy of state of the art prostheses. Image source: (Joudrie, 2014)

In fact, 3D printing has made prosthetics cheap enough that they can be efficiently sourced in places where they are needed most. Charities such as e-NABLING Ghana and The Open Hand Project are printing custom prostheses around the globe in response to immediate needs. The Open Hand Project logo, pictured below, is a cartoon version of their flagship project, the 3D printable hand pictured alongside it.

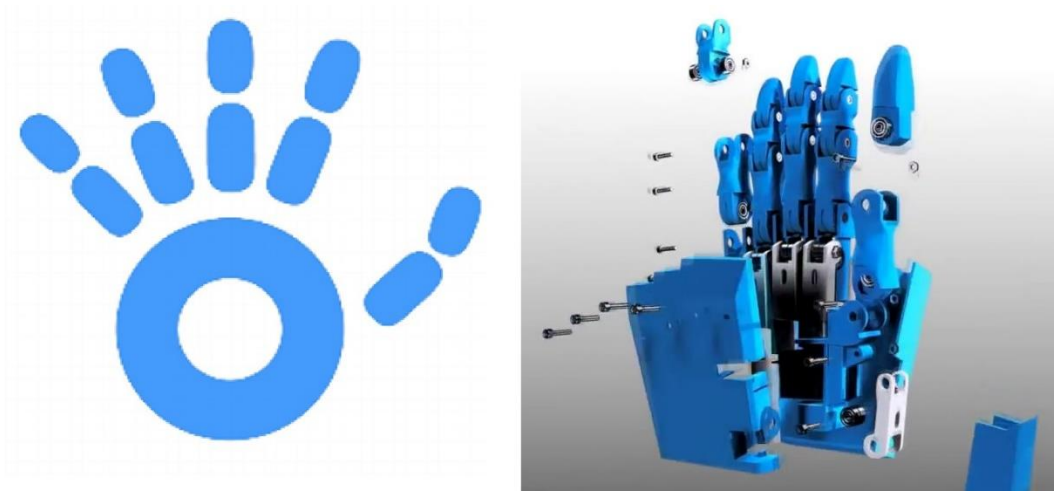

Figure 40: To the left, the Open Hand Project logo. To the right, an exploded view of the $50 3D printed hand "Dextrus" they hope to make available worldwide. Images adapted from openhandproject.org and gigazine.net

As the previous two figures show, there is a schism in the world of 3D printed prostheses between those who desire to make their products more extravagant and those who wish to make products that are more accessible. This duality is equally important for internal organ replacements as well as for external prosthetics, but it is much more noticeable for visible replacements. On the one hand, prettier prosthetics can help patients mentally accept their condition and help blend in with society, but on the other hand, people who cannot afford those versions should not be shamed for having basic devices. Similarly, more luxurious models could help float the costs

of developing better medical devices at the lower end of the spectrum, but this also depends on the developer making an effort to serve the full spectrum of needs.

In the world of internal organ replacements, 3D printing has not yet brachiated into higher and lower end models the way arms and legs have. Still, there is a gap between what people need and what most can afford. According to *Nature,* printed tissue replacements brought in $537 million in 2015[47], but that money had to come from patients who desperately needed it. In accordance with the laws of supply and demand, printed organs like the ears and bones like those discussed in *Nature* will cost as much as people are willing to pay for them.

4.2 Limitations of Available Printers

The two biggest limiting factors for 3D printers today are size and material. Every 3D printer has to be designed with these two factors in mind from the very beginning. After all, if the printed material can't be printed taller than 2cm, there is no point in building a printer that can move 100cm in the z-direction. Conversely, if the printer must be desktop sized and fast, it will never be able to accommodate a dozen different materials at once, or any that need extreme heat or air conditioning. As 3D printers get more efficient and more powerful (see section 5.2 below) these issues will be addressed, but they can never truly be resolved. Generally, these statements can be rearranged to say that the cost of a 3D printer will always reflect the quality of the build.

Nowhere are the trade-offs between capability and size more apparent than in the world of research bioprinters, a market segment completely dissociated from the

consumer market. The traditional rules of supply and demand are largely ignored by the boutique manufacturers that supply bioplotters to the well-funded research organizations that demand them. When EnvisionTEC rolled out its revolutionary 3D Bio-Printer it came with a modest price tag of $200,000, more than 10 times the price of a competitive desktop MakerBot. The second most well-known bioprinter is arguably the Organovo NovoGen MMX, a not-for-sale model whose product is 3D printed tissue sold to drug developers, according to *organovo.com*. Both of these products utilize syringe-based extrusion, just as the system designed as part of this project did. However, no current model is capable of printing larger than 30cm x 30cm as this printing system is designed to do. In fact, all current systems listed on *3dprintingindustry.com* for sale at less than $200,000 are designed to print in a Petri dish and have a total footprint of less than 50cm x 50cm. None provide their own sterility, unlike the printer designed in this report, which contains a novel laminar flow system.

4.3 Dynamic Elasticity Implants

With the incorporation of 3D printing into the tissue engineering field, it has become possible to use additive manufacturing techniques that other fields cannot replicate. One of the most novel, and perhaps most useful of these techniques, is the seamless interweaving of two or different materials in the structure of a scaffold[18]. Entwining different materials represents a step forward in the direction of fully programmable mechanical properties. Silk has the capability to be "programmed" with different properties, meaning it can be selectively treated to have higher stiffness in one area, or partially dissolve sacrificial layers and uncover time-

dependent functions[8]. But these examples pale in comparison to the ability to weave together silk and polylactic acid (PLA) together, for example. This ability gives rise to what can be called "dynamic elasticity implants," or in layman's terms, constructs whose properties are location-specific and span orders of magnitude. Compare the capability of a single structure to have intimately melded materials with the current gold standard total hip replacement (THR). In the image below, the different components of a THR are shown separately, just as they are before installation and after manufacturing. If instead, those parts could be printed together they could require half as many pieces, with one third as many interfaces. The fewer parts needed to fit together, the fewer opportunities there are for last-minute failures in the operating room and complications down the line that threaten the quality of life or the safety of the patient..

Figure 41: Components in a total hip replacement. Image source: http://www.hipandkneesurgery.ie/

Chapter 5 – Future Directions

5.1 Biocompatibility Studies

The largest unknown that remains for this printable hydrogel is whether they can be immediately adapted for cell printing. Assuming that cells are chosen based on their ability to withstand the high temperatures of the printing process, there are two main threats to their viability. The first is the concentration of reactive oxygen species released by riboflavin during illumination. The second is the hypertonic glycerol bath in which the hydrogel is submerged. Because these process steps occur simultaneously in this procedure, they are an even greater threat to the biocompatibility of the cells than they would be alone.

The first step towards understanding how well cells cope with these conditions will be a cell print test. Following the procedures outlined in other studies, the silk ink will be mixed with a cell line, such as 3T3 fibroblasts[57], and then undergo the complete printing process. Immediately after, the scaffold will be stained with calcein AM (a green fluorescent die absorbed by live cells) and ethidium homodimer (a red die concentrated in dead cells)[32]. The researcher will then use fluorescent imaging to analyze the scaffold and ImageJ software to count the number and density of living and dead cells.

$$Cell\ Viability = \frac{Number\ of\ living\ cells}{Total\ number\ of\ cells}\ x\ 100\%$$

Following the above formula, the cell viability in each image can be precisely calculated and averaged. The cell density, another important factor to track[78], is simply the number of cells per unit area in each image. Next, the scaffolds should be immersed in Dubelco's Mixed Eagle Media (DMEM), switched every 48 hours over

two weeks[30]. The cell viability and density at the one and two weeks mark should be compared to the baseline to ensure that cells can survive the entire process. Importantly, cell viability should increase after the initial printing as dead cells are washed away and new cells proliferate and divide in the scaffold[72]. In the same vein, the cell density should increase as the cells survive and divide in the scaffold.

If the cell viability data show that the cells are not thriving within the scaffold, it will take more experimentation to understand why. For example, if the dead cells are concentrated on the surface of the scaffold, it is likely that the glycerol bath is dehydrating the cells. This is distinct from the case where dead cells merely stick to the edge of the scaffold, in which case washing the scaffold should shear these cells from the structure. In order to reduce cell death from the glycerol bath, this step could be replaced with a longer bath at 300mM, a more neutral osmolarity that should not cause dehydration within the cells. Further still, the bath could be made from DMEM supplemented with glycerol. This would be a more expensive, but more biocompatible, solution that would cause gelling without dehydration and apoptosis.

The cytotoxicity from reactive oxygen species will be much more difficult to quench if it is found to be a lethal step. In which case, the first countermeasure would be to surround the ink with molecular oxygen in order to quench some of the reactive species[39]. Because this would also stop some of the polymers from gelling, this solution might weaken the gels and need to be compensated for with other measures. Alternatively, gelling the inks with lower power light for longer may reduce the peak oxygen concentration and keep more cells alive. Interestingly, it has been

reported that high fluence can also lead to reduced oxygen dispersion in some cases as the rapidly polymerizing hydrogel traps some oxygen species within the structure as it hardens[51]. In extreme cases, this can lead to bubble formation within the hydrogel and should be avoided[77].

Once it has been established that these hydrogels can be printed with cells safely inside, the next step is to attempt *in vivo* biocompatibility studies. Because rats are the standard first model for these studies[73], murine stem cells could be loaded into the scaffolds which would be surgically implanted into mice. After predetermined amounts of time, such as one week, four weeks, and six months, the scaffolds would be excised and examined for biodegradability and ingrowth[5]. Briefly, the tissue will be plasticized in parylene, sectioned into 5μm slides, and stained with hematoxylin and eosin to observe the cells and ECM in contrast with the silk scaffold. The goal would be to see the tissue scaffolds broken down by the host's immune system and replaced with stem cells and native tissue. A failed study would show immune rejection through fibrogenesis and encapsulation. In order to increase the compatibility between the scaffold and the host, proteins could be adsorbed to the surface of the gel, or the polymers themselves could be functionalized with peptides such as RGD to promote cell attachment[79].

Eventually, long-term studies will be needed to prove that these scaffolds can serve as the basis for organ replacement therapy. These studies would involve 3D scans of animal tissue, such as a tendon, 3D printing an exact replica, and replacing the healthy tissue with the printed scaffold seeded with stem cells. Eventually the tissue would be removed and the biocompatibility of the scaffold would be proven.

5.2 3D Printed Organ Replacements

Now that printing cells into basic geometries is a reality[3], printing independent living tissue is the next major breakthrough for additive manufacturing in medicine. While prosthetic implants can and have been 3D printed (see above), the holy grail of tissue engineering remains printing a functional organ such as the kidney or heart. The most important reason to attempt 3D printing organs is to address the tragically low rate of viable organ donations. The U.S. Department of Health and Human Services maintains an up-to-date list of the number of people needing lifesaving transplants and estimates that 22 people die every day waiting for one. It is commonly known that the number of transplants needed has been increasing for decades[47] but the number of organ donors has flatlined for at least the last 10 years.

Certain groups have found limited success in printing a prosthetic organ out of combinations of inorganic material. Paolo Macchiarini recently became famous, and then infamous, for his research in the field of tracheal implants using scaffolds seeded with stem cells sourced from his patients. Many people are also familiar with the famous photo of a rat growing a human ear on its back, but the scientists of the future hope to bypass the need for animal carriers in the first place. Writing in *Nature*, Heidi Ledford forecasts the use of printed hydrogels with cell ink to replace the need for conventional tissue replacement therapies. Current prognosticators are hopeful that simultaneous advances in material science, biology, and biomedical engineering will incrementally advance the abilities of doctors to replace organs as they die.

Figure 42: Rudimentary printed tissue replacements. The kidney organoid, top left, was printed with kidney cell inks. Source: Ledford, 2015

Early work in the field of whole organ printing has yielded rudimentary structures like those picture above. Clockwise form the top: ear scaffolds that could be regrown inside a bioreactor; metacarpals that could be implanted in a patient and replaced with human cells over time; and a kidney organoid with incorporated cells. Unfortunately, printing an entire organ is exponentially more difficult than printing a single tissue. The complexities of even a relatively simple organ like skin have prohibited even state-of-the-art printers from replicating its properties. As an example, the Objet 1000 Plus from Stratasys can print with 14 different materials simultaneously, but even though skin has only a handful of layers, no one has ever successfully printed a successful skin graft. This is not only because the material of the skin is difficult to print, but because the microscale features of the skin have to be precisely replicated at the macroscale. That level combination of accuracy and size has yet to be accomplished.

5.3 3D Printing in the Millimeter and Meter Scales

Printing both extremely fine and extremely large structures continues to be a difficult, expensive task that is better performed by traditional methods. Still, small hints of the capabilities to come can be seen even in today's basic use of 3D printing technology. Photolithography, for example, has been in use for creating computer chips from semiconductors and metals for decades. Light-based curing systems are spiritually similar to those studied in this report, although they are much more direct. Essentially, photopolymers absorb photons and use that energy to crosslink together, while un-linked polymers can be separated in a developing process[10]. It was long thought that the wavelength of the light used would be the lower limit on the resolution of photolithography, but various resolution-enhancing techniques were developed that have pushed the boundaries of photolithography to the point where today, 193nm light is used to imprint 10 nm transistors[54]. Interestingly, photopolymer materials are used all the way down to these single-nanometer devices and up to the meter scale as part of the "Major Lazer" and Massivit Gel Dispensed Printing (GPD) projects. According to *3ders.org*, the largest of these systems, the Massivit 3D printer pictured right, can print a car chassis or life-size statue.

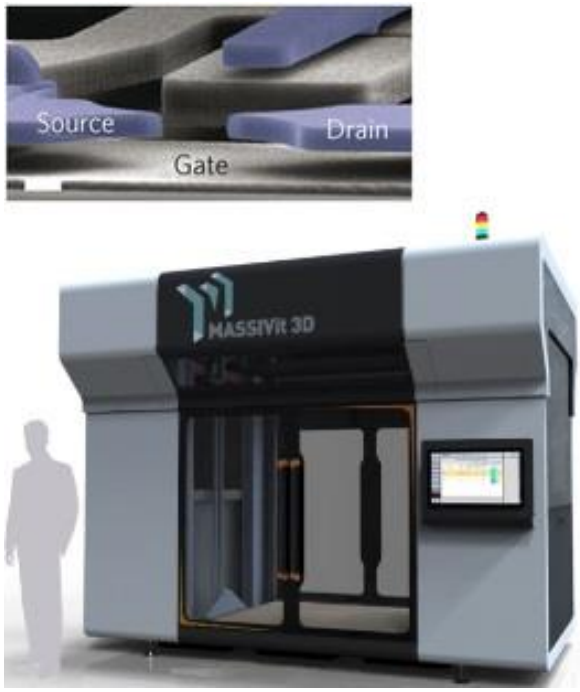

Figure 43: Size comparison of the smallest and largest structures "printed" with photolithography. Images adapted from (Muoth, 2010) and 3ders.org.

Large-scale rapid prototyping isn't limited to photopolymers. Some of the most innovative adaptions of these techniques are based on RepRap's fused filament fabrication (FFF) method. More than one company has experimented with printing entire buildings using printers that are essentially the scaffolding around the structure. At a certain point, the material itself is all that limits the size and speed of the printer. The stronger the material, the higher it can be built and the faster the printer can move. This line of thinking inspired the engineers of the Winsun Corporation in China to build a concrete printer that can print structures hundreds of cubic meters in volume in less than 24 hours. Several companies now boast the capability to print a small building, with at least a dozen capable of printing something at least the size of a car.

Figure 44: The nozzle of the 3D printer designed by the Winsun Corporation to print houses. Image source: mashable.com

Every step towards faster, better printers is a large stride toward a higher quality of living. Printing cells lead to printed tissues, which will lead to organ replacements, which will lead to fantastical treatments for conditions that are currently fatal.

Appendix A – Blue LED Illumination

The procedure for exposing samples to blue light was adapted from Chapter 6 of Matthew Applegate's Dissertation. Three blue LEDs with emission peaks at 450nm are placed in an equilateral triangle approximately 10cm above the surface of the gels. The measured radiant energy for one 60 minute exposure on a 35mm cylinder was 763 Joules. There was a large dependency on the angle of the exposure to the fluence so it was necessary to expose the inks within a narrow region in between all three LEDs. Additionally, each sample was flipped at the 30 minute mark to control for the opacity within the gel. After 90 minutes in the glycerol bath, the inks begin to whiten as the silk crosslinks and the gel forms. For this reason, 60 minutes was chosen as the cutoff time for illumination.

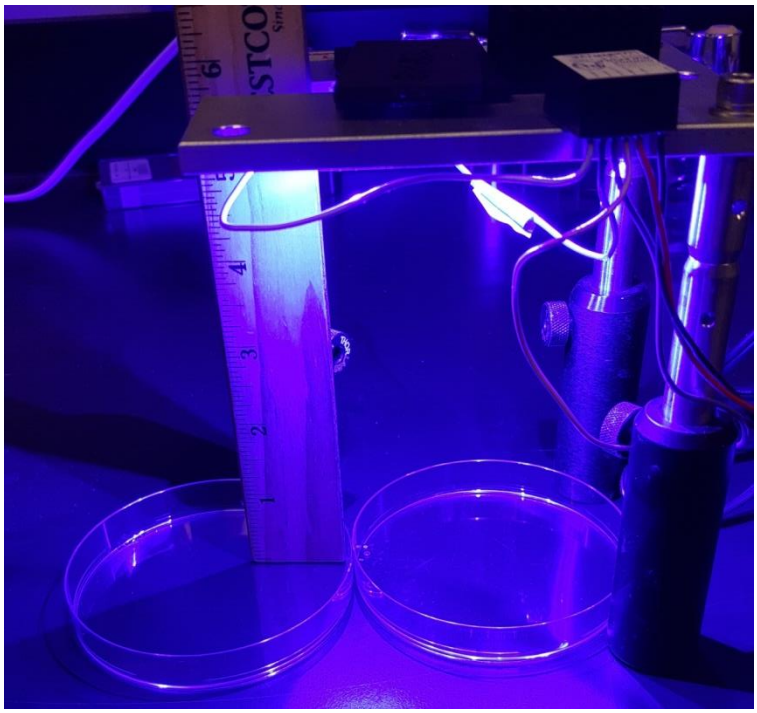

Figure 45: Blue light exposure setup

Appendix B – Statistics

A student license of Minitab 17 was acquired for use in all statistical analyses. The tests run to compare data were 2-sample t-tests and unless otherwise stated, p-values are considered significant if they are below 0.001, as 0.05 was found to be too generous a standard. For example, in comparing compression moduli from fifth cycle loading and from testing to failure, almost every possible combination of two data sets yielded a p-value below 0.05. Obviously it would not be helpful to identify or discuss "significant differences" between similar groups of data where common sense can rule out any possible meaning.

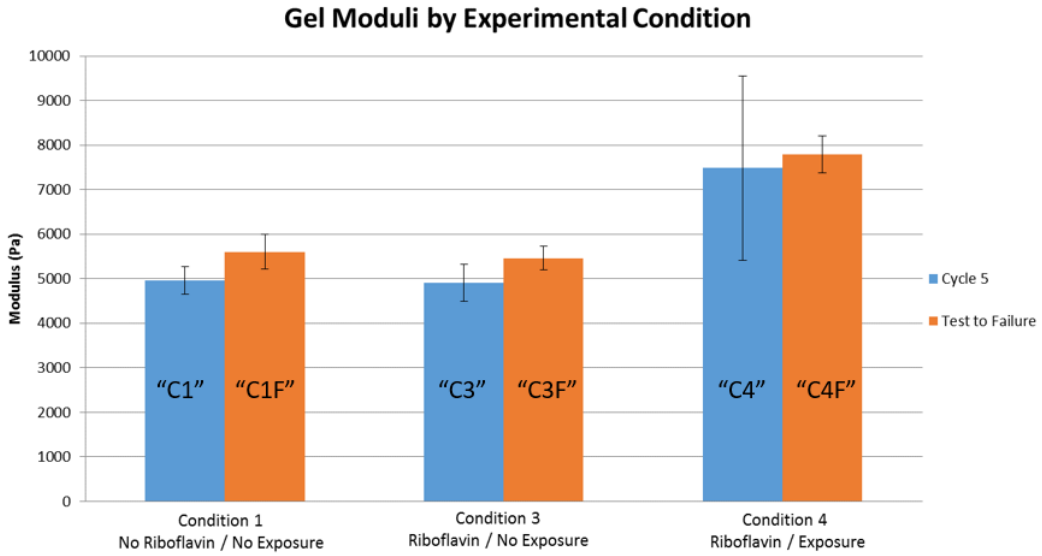

Figure 46: Gel moduli from failure testing and cycle 5 testing, compared.

Demonstration of Unhelpful P-Values						
	C1	C3	C4	C1F	C3F	C4F
C1						
C3	0.607					
C4	0.000	0.000				
C1F	0.010	0.005	0.000			
C3F	0.004	0.002	0.000	0.480		
C4F	0.000	0.000	0.503	0.000	0.000	

Table 6: Demonstration of Unhelpful P-values

Appendix C – Riboflavin Saturation

Unlike native forms of riboflavin, the phosphate salt version of riboflavin used in this study was a type II photoinitiator. For the purposes of this study, the most meaningful difference between the classes of photoinitiators is that type II chemicals are not catalysts but reactants in the process of forming free radicals. Given enough light, it must be theoretically possible to excite all the riboflavin within the ink and no benefit will come from further illumination. This saturation point was not thoroughly investigated in this report, but some condition 4 inks were made with a different batch of raw materials and exposed to three different amounts of light before being placed on a shaker in the dark for the remainder of the 2.5 hour glycerol bath. None of the moduli were significantly different from one another but in order they are: 12.3 ± 1.1kPa, 11.3 ± 1.1kPa, and 11.1 ± 1.3kPa. This data suggests that 300J of light is a lower bound for light saturation in condition 4 gels.

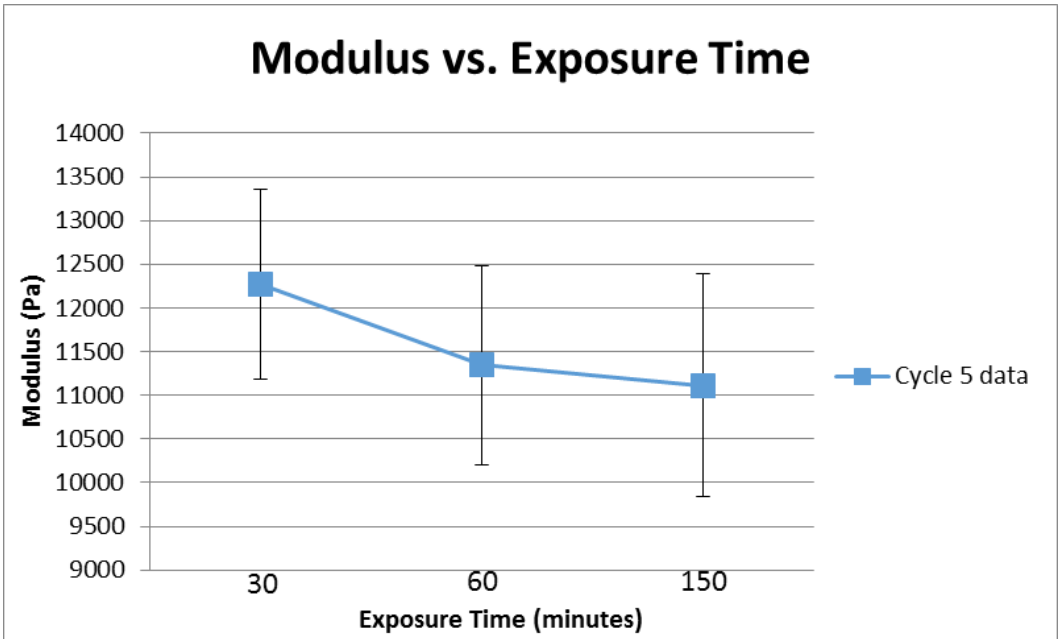

Figure 47: Change in modulus vs exposure time. The insignificant decrease is likely due to less time in the shaker after the riboflavin was saturated with light.

Bibliography

1. Achu, C., Byju, G., Kulkarni, A., & Gundiah, N. (n.d.). Mechanics of Gelatin and Elastin based hydrogels as Tissue Engineered.

2. Ahearne, M., Yang, Y., & Liu, K. (2008). Mechanical Characterisation of Hydrogels for Tissue Engineering Applications. *Tissue Engineering*, *4*, 1–16. Retrieved from http://www.oulu.fi/spareparts/ebook_topics_in_t_e_vol4/abstracts/ahearne.pdf

3. Ahearne, M., Yang, Y., El Haj, A. J., Then, K. Y., & Liu, K.-K. (2005). Characterizing the viscoelastic properties of thin hydrogel-based constructs for tissue engineering applications. *Journal of the Royal Society, Interface / the Royal Society*, *2*(5), 455–63. http://doi.org/10.1098/rsif.2005.0065

4. Ahmad, I., Iqbal, K., Sheraz, M. A., Ahmed, S., Mirza, T., Kazi, S. H., & Aminuddin, M. (2013). Photoinitiated polymerization of 2-hydroxyethyl methacrylate by riboflavin/triethanolamine in aqueous solution: a kinetic study. *ISRN Pharmaceutics*, *2013*, 958712. http://doi.org/10.1155/2013/958712

5. Andersen, M. Ø., Le, D. Q. S., Chen, M., Nygaard, J. V., Kassem, M., Bünger, C., & Kjems, J. (2013). Spatially controlled delivery of siRNAs to stem cells in implants generated by multi-component additive manufacturing. *Advanced Functional Materials*, *23*(45), 5599–5607. http://doi.org/10.1002/adfm.201300832

6. Ang, M. (2016, February 19). RepRap Improvements: A Collection by mangtronix. Retrieved March 02, 2016, from http://www.thingiverse.com/mangtronix/collections/reprap-improvements/page:1

7. Angelica, M. D., & Fong, Y. (2008). NIH Public Access. *October*, *141*(4), 520–529. http://doi.org/10.1016/j.surg.2006.10.010.Use

8. Applegate, M. B., Partlow, B. P., Coburn, J., Marelli, B., Pirie, C., Pineda, R., … Omenetto, F. G. (2016). Photocrosslinking of Silk Fibroin Using Riboflavin for Ocular Prostheses. *Advanced Materials*, n/a–n/a. http://doi.org/10.1002/adma.201504527

9. Bakarich, S. E., Gorkin III, R., in het Panhuis, M., & Spinks, G. M. (2014). Three-dimensional printing fiber reinforced hydrogel composites. *ACS applied materials & interfaces*, *6*(18), 15998-16006.

10. Beke, S., Anjum, F., Tsushima, H., Ceseracciu, L., Chieregatti, E., Diaspro, a., … Brandi, F. (2012). Towards excimer-laser-based stereolithography: a rapid

process to fabricate rigid biodegradable photopolymer scaffolds. *Journal of The Royal Society Interface*, *9*(76), 3017–3026. http://doi.org/10.1098/rsif.2012.0300

11. Bernt Melø, T., Adriana Ionescu, M., Haggquist, G. W., & Razi Naqvi, K. (1999). Hydrogen abstraction by triplet flavins. I: Time-resolved multi-channel absorption spectra of flash-irradiated riboflavin solutions in water. *Spectrochimica Acta - Part A: Molecular and Biomolecular Spectroscopy*, *55*(11), 2299–2307. http://doi.org/10.1016/S1386-1425(99)00097-9

12. Brandi, F., Anjum, F., Ceseracciu, L., Barone, a C., & Athanassiou, a. (2011). Rigid biodegradable photopolymer structures of high resolution using deep-UV laser photocuring. *Journal of Micromechanics and Microengineering*, *21*, 054007. http://doi.org/10.1088/0960-1317/21/5/054007

13. Carre, C., Decker, C., Fouassier, J. P., & Lougnot, D. J. (1990). Lasers and Photopolymers. *Laser Chem.*, *10*, 349–366.

14. Castro, N. J., O'Brien, J., & Zhang, L. G. (2015). Integrating biologically inspired nanomaterials and table-top stereolithography for 3D printed biomimetic osteochondral scaffolds. *Nanoscale*, *7*(33), 14010–22. http://doi.org/10.1039/c5nr03425f

15. Chao, P. G., Yodmuang, S., Wang, X., Sun, L., Kaplan, D. L., & Vunjak-Novakovic, G. (2010). Silk hydrogel for cartilage tissue engineering. *Journal of Biomedical Materials Research - Part B Applied Biomaterials*, *95*(1), 84–90. http://doi.org/10.1002/jbm.b.31686

16. Chatterjee, K., Lin-Gibson, S., Wallace, W. E., Parekh, S. H., Lee, Y. J., Cicerone, M. T., ... & Simon, C. G. (2010). The effect of 3D hydrogel scaffold modulus on osteoblast differentiation and mineralization revealed by combinatorial screening. *Biomaterials*, *31*(19), 5051-5062.

17. Chosewood, L. C., & Wilson, D. E. (2007). *Biosafety in microbiological and biomedical laboratories*. Diane Publishing.

18. Cloyd, J. M., Malhotra, N. R., Weng, L., Chen, W., Mauck, R. L., & Elliott, D. M. (2007). Material properties in unconfined compression of human nucleus pulposus, injectable hyaluronic acid-based hydrogels and tissue engineering scaffolds. *European Spine Journal*, *16*(11), 1892–1898. http://doi.org/10.1007/s00586-007-0443-6

19. Cox, T. R., & Erler, J. T. (2011). Remodeling and homeostasis of the extracellular matrix: implications for fibrotic diseases and cancer. *Disease Models and Mechanisms*, *4*(2), 165-178.

20. Crump, S. S. (1992). *U.S. Patent No. 5,121,329*. Washington, DC: U.S. Patent and Trademark Office.

21. Deckard, C. R. (1989). *U.S. Patent No. 4,863,538*. Washington, DC: U.S. Patent and Trademark Office.

22. De la garza, A. E., Vasquez, C. P., & Gonzalez, E. R. (2013, June 3). UV Curing with Lasers. Retrieved May 02, 2016, from http://www.adhesivesmag.com/articles/91983-uv-curing-with-lasers

23. Dhariwala, B., Hunt, E., Boland, T., & Ph, D. (2004). Rapid Prototyping of Tissue-Engineering Constructs , Using, *10*(9), 1316–1322.

24. Drössler, P., Holzer, W., Penzkofer, A., & Hegemann, P. (2002). pH dependence of the absorption and emission behaviour of riboflavin in aqueous solution. *Chemical Physics*, *282*(3), 429-439.

25. Ebert, L. C., Thali, M. J., & Ross, S. (2011). Getting in touch-3D printing in Forensic Imaging. *Forensic Science International*, *211*(1-3), 1–6. http://doi.org/10.1016/j.forsciint.2011.04.022

26. Encinas, M. V, Rufs, A. M., Bertolotti, S., & Previtali, C. M. (2001). Free Radical Polymerization Photoinitiated by Riboflavin / Amines . Effect of the Amine Structure. *Excited States*, (Figure 1), 2845–2847. http://doi.org/10.1021/ma001649r

27. Fawzy, A. S., Nitisusanta, L. I., Iqbal, K., Daood, U., & Neo, J. (2012). Riboflavin as a dentin crosslinking agent: Ultraviolet A versus blue light. *Dental Materials*, *28*(12), 1284–1291. http://doi.org/10.1016/j.dental.2012.09.009

28. Galloway, K. C., Polygerinos, P., Walsh, C. J., & Wood, R. J. (2013). Mechanically programmable bend radius for fiber-reinforced soft actuators. *Advanced Robotics (ICAR), 2013 16th International Conference on*, 1–6. http://doi.org/10.1109/ICAR.2013.6766586

29. Hajeer, M. Y., Millett, D. T., Ayoub, A. F., & Siebert, J. P. (2004). Current Products and Practices: Applications of 3D imaging in orthodontics: Part I.*Journal of orthodontics*, *31*(1), 62-70.

30. Hockaday, L. A., Kang, K. H., Colangelo, N. W., Cheung, P. Y. C., Duan, B., Malone, E., … Butcher, J. T. (2012). Rapid 3D printing of anatomically accurate and mechanically heterogeneous aortic valve hydrogel scaffolds. *Biofabrication*, *4*(3), 035005. http://doi.org/10.1088/1758-5082/4/3/035005

31. Hull, C. W. (1986). *U.S. Patent No. 4,575,330*. Washington, DC: U.S. Patent and Trademark Office.

32. Ibusuki, S., Halbesma, G. J., Randolph, M. A., Redmond, R. W., Kochevar, I. E., & Gill, T. J. (2007). Photochemically cross-linked collagen gels as three-dimensional scaffolds for tissue engineering. *Tissue Engineering*, *13*(8), 1995–2001. http://doi.org/10.1089/ten.2006.0153

33. Imlay, J. A., & Linn, S. (1988). DNA damage and oxygen radical toxicity.*Science*, *240*(4857), 1302-1309.

34. Jacobs, S., Grunert, R., Mohr, F. W., & Falk, V. (2008). 3D-Imaging of cardiac structures using 3D heart models for planning in heart surgery: a preliminary study. *Interactive cardiovascular and thoracic surgery*, *7*(1), 6-9.

35. Jeng, J. Y., Wong, Y. S., & Ho, C. T. (2001). Curing characteristics of the photopolymer used in the solid laser-diode plotter RP system. *The International Journal of Advanced Manufacturing Technology*, *17*(7), 535-542.

36. Jones, R., Haufe, P., Sells, E., Iravani, P., Olliver, V., Palmer, C., & Bowyer, A. (2016). RepRap – the replicating rapid prototyper RepRap – the replicating rapid prototyper, (January 2011), 177–191. http://doi.org/10.1017/S026357471000069X

37. Joudrie, K., & Thinking Robot Studios. (2014). 3D Printing Makes Thinkers into Doers. Retrieved March 29, 2016, from https://www.3dsystems.com/sites/www.3dsystems.com/files/cs-novascotia_prosthetic-final.pdf

38. Kang, L. H., Armstrong, P. A., Lee, L. J., Duan, B., Kang, K. H., & Butcher, J. T. (2016). Optimizing Photo-Encapsulation Viability of Heart Valve Cell Types in 3D Printable Composite Hydrogels. *Annals of Biomedical Engineering*. http://doi.org/10.1007/s10439-016-1619-1

39. Kato, Y., Uchida, K., & Kawakishi, S. (1994). Aggregation of collagen exposed to UVA in the presence of riboflavin: a plausible role of tyrosine modification. *Photochemistry and Photobiology*, *59*(3), 343–349. http://doi.org/10.1111/j.1751-1097.1994.tb05045.x

40. Kim, S. H., & Chu, C. C. (2009). Visible light induced dextran-methacrylate hydrogel formation using (-)-riboflavin vitamin B2 as a photoinitiator and L-arginine as a co-initiator. *Fibers and Polymers*, *10*(1), 14–20. http://doi.org/10.1007/s12221-009-0014-z

41. Kim, U. J., Park, J., Joo Kim, H., Wada, M., & Kaplan, D. L. (2005). Three-dimensional aqueous-derived biomaterial scaffolds from silk fibroin. *Biomaterials*, *26*(15), 2775–2785. http://doi.org/10.1016/j.biomaterials.2004.07.044

42. Kim, U. J., Park, J., Li, C., Jin, H. J., Valluzzi, R., & Kaplan, D. L. (2004). Structure and properties of silk hydrogels. *Biomacromolecules*, *5*(3), 786–792. http://doi.org/10.1021/bm0345460

43. Klyce, S. D. (2013). UVA-riboflavin collagen cross-linking: A misnomer perhaps, but it works! *Investigative Ophthalmology and Visual Science*, *54*(3), 1635. http://doi.org/10.1167/iovs.13-11807

44. Knezevic, A., Ristic, M., Demoli, N., Tarle, Z., Music, S., & Mandic, V. N. (2007). Composite photopolymerization with diode laser. *Operative dentistry*,*32*(3), 279-284.

45. Kotaki, A., Naoi, M., Okuda, J., & Yagi, K. (1967). Absorption and fluorescence spectra of riboflavin tetrabutyrate in various solvents. *Journal of biochemistry*, *61*(3), 404-406.

46. Koziol, J. (1965). Absorption Spectra of Riboflavin, Lumiflavin, and Lumichrome in Organic Solvents - Brevi comunicazioni - Brief Reports, 189–190.

47. Ledford, H. (2015). Printed body parts come alive. *Nature*, *520*(7547), 273. http://doi.org/10.1038/520273a

48. Lovell, L. G., Lu, H., Elliott, J. E., Stansbury, J. W., & Bowman, C. N. (2001). The effect of cure rate on the mechanical properties of dental resins. *Dental Materials*, *17*(6), 504–511. http://doi.org/10.1016/S0109-5641(01)00010-0

49. Lu, Y. (2006). *Micro/nano fabrication of polymeric materials by DMD-based micro-stereolithography and photothermal imprinting*. p. 35 ProQuest.

50. Mainster, M. A., Ham, W. T., & Delori, F. C. (1983). Potential Retinal Hazards. *Ophthalmology*, *90*(8), 927–932. http://doi.org/10.1016/S0161-6420(83)80019-0

51. McCall, A. S., Kraft, S., Edelhauser, H. F., Kidder, G. W., Lundquist, R. R., Bradshaw, H. E., … Conrad, G. W. (2010). Mechanisms of Corneal Tissue Cross-linking in Response to Treatment with Topical Riboflavin and Long-Wavelength Ultraviolet Radiation (UVA). *Investigative Opthalmology & Visual Science*, *51*(1), 129. http://doi.org/10.1167/iovs.09-3738

52. Metscher, B. D. (2009). MicroCT for comparative morphology: simple staining methods allow high-contrast 3D imaging of diverse non-mineralized animal tissues. *BMC Physiology*, *9*(11), 1–14. http://doi.org/10.1186/1472-6793-9-11

53. Millsaps, B. B. (2015, March 10). Japan's Fasotec Creates Realistic 3D Printed 'Biotexture Wet Models' for Surgical Training. Retrieved March 28, 2016, from http://3dprint.com/49992/fasotec-3d-print-wet-model/

54. Muoth, M., Helbling, T., Durrer, L., Lee, S. W., Roman, C., & Hierold, C. (2010). Hysteresis-free operation of suspended carbon nanotube transistors.*Nature Nanotechnology*, *5*(8), 589-592.Naoi, M., Okuda, J. U. N., & Yagi, K. (1967). N o t e s, *61*(3).

55. Ohya, S., Kidoaki, S., & Matsuda, T. (2005). Poly(N-isopropylacrylamide) (PNIPAM)-grafted gelatin hydrogel surfaces: Interrelationship between

microscopic structure and mechanical property of surface regions and cell adhesiveness. *Biomaterials*, *26*(16), 3105–3111. http://doi.org/10.1016/j.biomaterials.2004.08.006

56. Orthodontist, T. A. (2000). Current Products and Practice, *3125*(March), 335–338. http://doi.org/10.1179/146531205225021807

57. Ovsianikov, A., M??hleder, S., Torgersen, J., Li, Z., Qin, X. H., Van Vlierberghe, S., … Stampfl, J. (2014). Laser photofabrication of cell-containing hydrogel constructs. *Langmuir*, *30*(13), 3787–3794. http://doi.org/10.1021/la402346z

58. Pan, H. M., Seuss, M., Neubauer, M. P., Trau, D. W., & Fery, A. (2016). Tuning the Mechanical Properties of Hydrogel Core–Shell Particles by Inwards Interweaving Self-Assembly. *ACS Applied Materials & Interfaces*, *8*(2), 1493–1500. http://doi.org/10.1021/acsami.5b10886

59. Partlow, B. P., Hanna, C. W., Rnjak-Kovacina, J., Moreau, J. E., Applegate, M. B., Burke, K. A., … Kaplan, D. L. (2014). Highly tunable elastomeric silk biomaterials. *Advanced Functional Materials*, *24*(29), 4615–4624. http://doi.org/10.1002/adfm.201400526

60. Rajaram, A., Schreyer, D. J., & Chen, D. X. B. (2015). Use of the polycation polyethyleneimine to improve the physical properties of alginate-hyaluronic acid hydrogel during fabrication of tissue repair scaffolds. *Journal of Biomaterials Science. Polymer Edition*, *5063*(March), 1–23. http://doi.org/10.1080/09205063.2015.1016383

61. Rich, H., Odlyha, M., Cheema, U., Mudera, V., & Bozec, L. (2014). Effects of photochemical riboflavin-mediated crosslinks on the physical properties of collagen constructs and fibrils. *Journal of Materials Science: Materials in Medicine*, *25*(1), 11–21. http://doi.org/10.1007/s10856-013-5038-7

62. Rioux, M. (1994). 3-D Imaging: Theory and Applications, *2350*, 2–15.

63. Rockwood, D. N., Preda, R. C., Yücel, T., Wang, X., Lovett, M. L., & Kaplan, D. L. (2011). Materials fabrication from Bombyx mori silk fibroin. *Nature Protocols*, *6*(10), 1612–1631. http://doi.org/10.1038/nprot.2011.379

64. Rueggeberg, F. A. (2002). From vulcanite to vinyl, a history of resins in restorative dentistry. *Journal of Prosthetic Dentistry*, *87*(4), 364–379. http://doi.org/10.1067/mpr.2002.123400

65. Santis, R. De, Causa, F., Sarracino, F., Netti, P. A., & Ambrosio, L. (2004). Biomimetic Composite Hydrogels for Tissue Reconstruction Abstract : Acknowledgements :, *9*(1), 7–10.

66. Segurola, J., Allen, N. S., Edge, M., & Mahon, A. M. (1999). Design of eutectic photoinitiator blends for UV/visible curable acrylated printing inks and coatings. *Prog. Org. Coat.*, *37*(1-2), 23–27. http://doi.org/10.1016/S0300-9440(99)00052-1

67. Small, D. M., Sanchez, W. Y., Hickey, M. J., & Gobe, G. C. (2014). Multiphoton fluorescence microscopy of the live kidney in health and disease Multiphoton fluorescence microscopy of the live kidney in health and disease. *Journal of Biomedical Optics*, *19*(2), 020901. http://doi.org/10.1117/1

68. Specimens, P. (2008). Compressive Properties of Rigid Plastics 1. *Annual Book of ASTM Standards*, *i*, 1–8. http://doi.org/10.1520/D0695-15.2

69. Statista. (n.d.). 3D printing market value 2011-2021 | Forecast. Retrieved February 23, 2016, from http://www.statista.com/statistics/261693/3d-printing-market-value-forecast/

70. Stowers, R. S., Allen, S. C., & Suggs, L. J. (2015). Dynamic phototuning of 3D hydrogel stiffness. *Proceedings of the National Academy of Sciences of the United States of America*, *112*(7), 1953–1958. http://doi.org/10.1073/pnas.1421897112

71. Tabriz, A. G., Hermida, M. A., Leslie, N. R., & Shu, W. (2015). Three-dimensional bioprinting of complex cell laden alginate hydrogel structures. *Biofabrication*, *7*(4), 045012. http://doi.org/10.1088/1758-5090/7/4/045012

72. Tehfe, M., Louradour, F., Lalevée, J., & Fouassier, J.-P. (2013). Photopolymerization Reactions: On the Way to a Green and Sustainable Chemistry. *Applied Sciences*, *3*(2), 490–514. http://doi.org/10.3390/app3020490

73. Toma, C., Pittenger, M. F., Cahill, K. S., Byrne, B. J., & Kessler, P. D. (2002). Human mesenchymal stem cells differentiate to a cardiomyocyte phenotype in the adult murine heart. *Circulation*, *105*(1), 93-98.

74. Tyagi, A., & Penzkofer, A. (2010). pH dependence of the absorption and emission behavior of lumiflavin in aqueous solution. *J. of Photochemistry and Photobiology A: Chemistry*, *215*, 108–117.

75. Udupa, J. K., & Herman, G. T. (Eds.). (1999). *3D imaging in medicine*. CRC press.

76. Wang, T., Bruin, G. J., Kraak, J. C., & Poppe, H. (1991). Preparation of Polyacrylamide Gel-Fillled Fused Sillica Capillaries by Photopolymerization with Riboflavin as the Initiator. *Anal. Chem*, *63*, 2207–2208.

77. Wang, Z., Jin, X., Dai, R., Holzman, J. F., & Kim, K. (2016). An ultrafast hydrogel photocrosslinking method for direct laser bioprinting. *RSC Adv.*, *6*(25), 21099–21104. http://doi.org/10.1039/C5RA24910D

78. Wollensak, G., Spoerl, E., & Seiler, T. (2003). Riboflavin/ultraviolet-A-induced collagen crosslinking for the treatment of keratoconus. *American Journal of Ophthalmology*, *135*(5), 620–627. http://doi.org/10.1016/S0002-9394(02)02220-1

79. Yodmuang, S., McNamara, S. L., Nover, A. B., Mandal, B. B., Agarwal, M., Kelly, T. A. N., … Vunjak-Novakovic, G. (2015). Silk microfiber-reinforced silk hydrogel composites for functional cartilage tissue repair. *Acta Biomaterialia*, *11*(1), 27–36. http://doi.org/10.1016/j.actbio.2014.09.032

80. Zayat, M., Garcia-Parejo, P., & Levy, D. (2007). Preventing UV-light damage of light sensitive materials using a highly protective UV-absorbing coating.*Chemical Society Reviews*, *36*(8), 1270-1281.

81. Zhang, W., Wang, X., Wang, S., Zhao, J., Xu, L., Zhu, C., … Jiang, X. (2011). The use of injectable sonication-induced silk hydrogel for VEGF 165 and BMP-2 delivery for elevation of the maxillary sinus floor. *Biomaterials*, *32*(35), 9415–9424. http://doi.org/10.1016/j.biomaterials.2011.08.047

82. Žukauskas, A., Bataviciute, G., Sciuka, M., Balevicius, Z., Melninkaitis, A., & Malinauskas, M. (2015). Effect of the photoinitiator presence and exposure conditions on laser-induced damage threshold of ORMOSIL (SZ2080). *Optical Materials*, *39*(April), 224–231. http://doi.org/10.1016/j.optmat.2014.11.031